Abiotic and seasonal control of soil-produced CO_2 efflux in karstic ecosystems located in Oceanic and Mediterranean climates

Elena Garcia-Anton[1], Soledad Cuezva[1,2], Angel Fernandez-Cortes[3], Miriam Alvarez-Gallego[1], Concepcion Pla[4], David Benavente[5], Juan Carlos Cañaveras[5], Sergio Sanchez-Moral[1]

[1] Department of Geology, National Museum of Natural Sciences (MNCN-CSIC), 28006 Madrid, Spain. elena.garcia@mncn.csic.es, scuezva@mncn.csic.es, mag@mncn.csic.es, ssmilk@mncn.csic.es
[2] Geomnia Natural Resources SLNE, 28003 Madrid, Spain.
[3] Department of Biology and Geology, University of Almeria, 04120 Almeria, Spain. acortes@ual.es
[4] Department of Civil Engineering, University of Alicante, San Vicente del Raspeig, 03690 Alicante, Spain. c.pla@ua.es
[5] Department of Environment and Earth Sciences, University of Alicante, San Vicente del Raspeig, 03690 Alicante, Spain. david.benavente@ua.es, jc.canaveras@ua.es

Abstract

This study characterizes the processes involved in seasonal CO_2 exchange between soils and shallow underground systems and explores the contribution of the different biotic and abiotic sources as a function of changing weather conditions. We spatially and temporally investigated five karstic caves across the Iberian Peninsula, which presented different microclimatic, geologic and geomorphologic features. The locations present Mediterranean and Oceanic climates. Spot air sampling of CO_2 (g) and $\delta^{13}CO_2$ in the caves, soils and outside atmospheric air was periodically conducted. The isotopic ratio of the source contribution enhancing the CO_2 concentration was calculated using the Keeling model. We compared the isotopic ratio of the source in the soil ($\delta^{13}C_s$–soil) with that in the soil-underground system ($\delta^{13}C_s$–system). Although the studied field sites have different features, we found common seasonal trends in their values, which suggests a climatic control over the soil air CO_2 and the $\delta^{13}CO_2$ of the sources of CO_2 in the soil ($\delta^{13}C_s$–soil) and the system ($\delta^{13}C_s$–system). The roots respiration and soil organic matter degradation are the main source of CO_2 in underground environments, and the inlet of the gas is mainly driven by diffusion and advection. Drier and warmer conditions enhance soil-exterior CO_2 interchange, reducing the CO_2 concentration and increasing the $\delta^{13}CO_2$ of the soil air. Moreover, the isotopic ratio of the source of CO_2 in both the soil and the system tends to heavier values throughout the dry and warm season.

We conclude that seasonal variations of soil CO_2 concentration and its $^{13}C/^{12}C$ isotopic ratio are mainly regulated by thermo-hygrometric conditions. In cold and wet seasons, the increase of soil moisture reduces soil diffusivity and allows the storage of CO_2 in the subsoil. During dry and warm seasons, the evaporation of soil water favours diffusive and advective transport of soil-derived CO_2 to the atmosphere. The soil CO_2 diffusion is enough important during this season to modify the isotopic ratio of soil produced CO_2 (3-6‰ heavier). Drought induces release of CO_2 with an isotopic ratio heavier than produced by organic sources. Consequently, climatic conditions drive abiotic processes that turn regulate a seasonal storage of soil-produced CO_2 within soil and underground systems. The results here obtained imply that abiotic emissions of soil-produced CO_2 must be an inherent consequence of droughts, which intensification has been forecasted at global scale in the next 100 years.

Keywords: Vadose Zone, CO_2 exchange, $\delta^{13}CO_2$, Climatic control, Soil CO_2 diffusion

1 Introduction

Climate change is expected to modify current climate producing not only a progressive global warming but also changes on the frequency, the severity and the nature of the climatic extreme events. Current climate models forecast a global intensification of heavy precipitation events, heat extremes and longer and stronger droughts (Ciais et al., 2013). This may produce substantial changes in the ecosystems affecting therefore to carbon cycling and its feedbacks to the climate system. There are still many uncertainties related to the processes controlling ecosystem carbon fluxes. Thus, responses of the environment to climate changes have not yet been completely determined in terms of time, direction or intensity (Frank et al., 2015).

Diverse climate-dependent processes occurring on different timescales (i.e., from hours to millions of years) are involved in ecosystems carbon cycling (Berner, 2003). Among them, carbonate weathering and underground CO_2 storage are abiotic processes that are considered significant parts of the terrestrial flux of carbon at short time scales (hourly, daily and annually

(Liu and Zhao, 2000; Mörner and Etiope, 2002; Kowalski et al., 2008; Gilfillan et al., 2009; Serrano-Ortiz et al., 2010; Roland et al., 2013; Fernandez-Cortes et al., 2015a)). Part of these carbon fluxes takes place in the subsoil vadose zone in which aqueous and gaseous transference processes of CO_2 between the underground environment and the overlying soil are regulated essentially by the temperature and water content of the soil-rock layer (Cuezva et al., 2011; Pla et al., 2017a).

Subsurface caves in the vadose zone commonly present high concentration of CO_2 compared to outdoor air. The main source of the CO_2 in the caves results from the organic activity taking place in the overlying soil (Baldini et al., 2006; Genty et al., 2008, Fig. 1) and/or the vadose zone (Noronha et al., 2015; Mattey et al., 2016). Soil CO_2 efflux is the largest terrestrial flux of CO_2, known as soil respiration (Ryan and Law, 2005; Jassal et al., 2007). Moreover, lately studies have identified an important source of CO_2 in caves in the decay of soil organic matter washed down into the unsaturated zone (Mattey et al., 2016). The transfer of organic-derived CO_2 towards less concentrated zones and throughout the system of air-filled pores, cracks and voids in bedrock is favoured by the diffusive mechanism (mass transport process) triggered as a response to the concentration gradient (Christoforou et al., 1996; Bourges et al., 2001; Breecker et al., 2012; Garcia-Anton et al., 2014a). Additionally, advection (bulk air movement) has been observed to be an important mechanism of CO_2 transport throughout some underground environments (Frisia et al., 2011; Fernandez-Cortes et al. 2015a; Mattey et al., 2016). Organic derived CO_2 also can reach the cave by geochemical dissolution in infiltrating water and afterward degassing in the underground environment (Fig. 1). This process is linked to speleothems formation. Nevertheless, several important studies concluded that CO_2 supply by dripping waters in caves is relatively low compared to the soil-derived CO_2 inlet in gaseous phase (Baldini et al., 2006; Frisia et al., 2011; Breecker et al., 2012).

The CO_2 stored in caves commonly presents variations strongly driven by ventilation (advective air movement) due to the inflow of less concentrated exterior air and the simultaneous outflow of the underground air (Fernandez-Cortes et al., 2009; Frisia et al., 2011; Garcia-Anton et al., 2014a, Fig. 1). Ventilation episodes are regulated by synoptic weather conditions (Bourges et al., 2001; Mattey et al., 2010; Fernandez-Cortes et al., 2011; Fernandez-Cortes et al 2015a, among others). Rainfall and the relative humidity of air regulate the water content in soil and host rock porous media that play important roles in regulating the gas exchange between the underground environment and the surface (Cuezva et al., 2011; Fernandez-Cortes et al., 2013). Air density contrasts (controlled by temperature gradient between the cave air and the atmosphere) and cave geometry determine the advective movement of air that produces the cave ventilation (Fernandez-Cortes et al., 2009; Faimon et al., 2012; Sanchez-Cañete et al., 2013; James et al., 2015). Interior temperature of caves is in general very stable compared to the exterior air due to the characteristic low thermal conductivity of rocks. This generates significant interior-exterior temperature contrasts that trigger ventilation and air exchange processes. On the other hand, caves morphology determines the inner-outer air masses altitudinal relationship, which in most of the cases determines caves ventilation patterns throughout the year (Faimon et al., 2012). Ventilation of caves releases the stored underground air that can influence seasonal and daily CO_2 fluxes between soil-subsoil and the atmosphere at local scale (Kowalski et al., 2008; Sanchez-Cañete et al., 2011; Hamerlynck et al., 2013; Chen et al., 2014; Wang et al., 2014). Discriminating the biogeochemical processes occurring through the rock and soil involving CO_2 is key to understanding the surface-atmosphere exchange of CO_2 in terrestrial ecosystems. The $\delta^{13}C$ of CO_2 ($\delta^{13}CO_2$) in air has been traditionally studied to identify the characteristic $\delta^{13}CO_2$ of ecosystem respiration and the contribution of different biotic or abiotic sources (Yakir and Sternberg, 2000; Pataki et al., 2003; Hemming et al., 2005). The isotopic ratio characterizes the chemical changes undergone by the gas, introducing identifiers for the source of production and transport mechanisms

(Maseyk et al., 2009; Kayler et al., 2010; Moyes et al., 2010; Bowling and Massman 2011; Shanhun et al., 2012; Garcia-Anton et al., 2014a). In studies carried out in natural environments, the $\delta^{13}CO_2$ of the source contributing to enhance the CO_2 concentration in air can be easily obtained by mass-balance estimations such as the Keeling approach (Keeling, 1958; Keeling, 1961). Traditionally, the Keeling plot has been used to identify the $\delta^{13}CO_2$ of a single source component contributing to the ecosystem. However, in this work, we applied the Keeling plot to study the interaction between three components of a karst system: exterior atmosphere, soil air and subsurface stored air. The data treatment applied highlights the differences between the isotopic ratio characterizing the soil contribution and the isotopic ratio corresponding to the combination of the soil and the underground system contribution.

The aim of the present research is to characterize biotic and abiotic processes involved in CO_2 exchange in the underground-soil-atmosphere system at the seasonal/annual scale. We examine the role of the vadose zone influencing ecosystem CO_2 fluxes as function of climate changes. We spatially and temporally investigated five karstic locations across the Iberian Peninsula with different geologic and geomorphologic features located at Oceanic and Mediterranean climates. The different locations gave us a broad view of the response of the systems to a range of conditions: from extremely hot and dry (Mediterranean climate summers) to temperate and humid (Oceanic climate). We focused our study on the variability of the isotopic signal $\delta^{13}C$ of the source of CO_2. Spot air sampling of CO_2 (g) and $\delta^{13}CO_2$ of the three major air masses involved (cave, soil and outside atmosphere) was periodically conducted (monthly and bimonthly). The main environmental conditions at the surface (temperature, relative humidity and rainfall) and inside the cave atmosphere (temperature, relative humidity and gases concentration in the air) were continuously measured and registered by monitoring systems during the sampling periods at each field site.

2. Sites, materials and methodology

2.1 Field sites

The studied sites are different caves located in the Iberian Peninsula (Fig. 2) that present different geologic, morphologic and climatic conditions. Different features of the studied caves are suitable to both identify common processes occurring in underground environments and distinguish them from local effects. Table 1 synthesizes relevant available information about the field sites.

2.1.1 Altamira

Altamira cave is a shallow vadose karst cavity located in a hill 161 m.a.s.l. at a depth of 322 m (8 m on average) below the surface (Fig. 3). The cavity has a single entrance in a topographically higher position (152 m.a.s.l.) and includes several main rooms that have a downward trend from the outside access to the deepest part of the cave. The host rock in the Altamira Cave is a thin to medium, parallel bedded, Cenomanian (Upper Cretaceous) limestone succession from 13.5 to 15 m thick.

Altamira cave is located in an Oceanic or specifically Warm temperate climate, fully humid with a temperate summer (Cfb climate type, Köppen-Geiger Classification slightly modified, AEMET-IM, 2011, Fig. 2, Table 1). The annual precipitation is approximately 1400 mm and the mean annual temperature and relative humidity are approximately 14 ^{o}C and 85%, respectively.

The cave was defined in Cuezva et al., (2009) as a stable environment, with high thermo-hygrometric stability throughout the year (ranges of monthly average temperatures: 13.38-14.56 ^{o}C, Garcia-Anton et al., 2014b) and a low energy exchange with the surface. Relatively high levels of air CO_2 are registered during winter and lowest values during summer (from June to October), due to the most effective cave ventilation in this warmer and drier period (ranges CO_2 concentrations: 677-5576 ppm, Garcia-Anton et al., 2014b). The characteristic ventilation pattern in this cave contrasts to the classical models (Mangin and Andrieux, 1988), in which

downward caves with a unique entrance in its upmost part are expected to present their ventilation stage during the winter (according to the inner-outer density/temperature gradient). Therefore, the cave must have unknown connections to the surface that allow active chimney-effect air movements during the summer. These connections have been identified in previous studies (Garcia-Anton et al., 2014a) and located in the lowest part of the cave (Well Hall, Fig. 3).

Water supply in this cave is relatively low and restricted to seepage waters. Maximum infiltration rates occur during autumn and winter, and occasionally during spring, whereas practically null percolation rates characterize the summer season (Cuezva, 2008). Consequently, speleothem development is scarce in this cave.

2.1.2 Castañar de Ibor

Castañar de Ibor cave is hosted in Neoproterozoic rocks that form the core of the Ibor Anticline. These rocks are shales and greywackes with interbedded dolostones and magnesites (Alonso-Zarza et al., 2011). The cave was developed by the dissolution of the dolomitic beds. Besides, the extensive weathering of the shales and greywackes favours collapses, which created and enlarged the cave. Castañar de Ibor cave exhibits a maze pattern with a labyrinthine distribution of galleries that indicates a strong structural and lithological control on its formation (Fig. 4). The cave entrance is currently a vertical access, 9 m long over an area of 1.5 m^2, with a quasi-hermetic trap door installed at the entrance.

The geographical area is characterized by a Mediterranean or specifically Warm temperate climate with a dry and hot summer (Csa climate type, Köppen-Geiger Classification slightly modified, AEMET-IM, 2011, Fig. 2, Table 1). The annual precipitation is relatively low (slightly above 500 mm/year) with long periods of drought and maximum rainfall in autumn. Mean annual temperature is 15.5^{o}C.

The Castañar de Ibor cave is a low energy and quite isolated cave with very high thermal stability throughout the annual cycle under natural conditions (monthly- averaged temperatures and CO_2 concentrations range 16.93-16.96 ^{o}C and 3364-3866 ppm, respectively, Fernandez-Cortes et al., 2011). The high stability on the climate conditions of the Castañar de Ibor cave is due to the scarce interchange with the exterior air, mainly driven by natural barometric fluxes (Fernandez-Cortes et al., 2011). This type of microclimate is characteristic of cavities relatively well connected with exterior, with a single small entrance located above the cave (Choppy, 1982).

Water inlet in the cave from exterior is restricted to slow infiltration that feed three small lakes (Fernandez-Cortes et al., 2010; Garcia-Guinea et al., 2013). This cave is especially remarkable by the quantity and variety of speleothems. Massive speleothems are associated with main fractures and bedding planes, while branching and fibrous, mostly aragonite, speleothems are related with capillary seepage or drip water (Alonso-Zarza et al., 2011).

2.1.3 Ojo Guareña

Ojo Guareña karst system is hosted in Upper Cretaceous limestones and dolomitic limestones (Camacho et al., 2006). In this geographic area, the climate is Oceanic or specifically Warm temperate climate, fully humid with a temperate summer (Cfb climate type, Köppen-Geiger Classification slightly modified, AEMET-IM, 2011, Fig. 2, Table 1). The annual mean precipitation is approximately 640 mm, and the average annual temperature is 11.9 ^{o}C (Fernandez-Cortes et al., 2015b).

The Ojo Guareña cave system, one of the longest cave systems in Europe with over 100 km of development, is distributed over several overlapping levels composed of passages up to 10 m high and 20 m wide with 3 main entrances and several other minor cavities. In the sinkhole plain, we can find several entrances to the subterranean karst system, such as the Palomera doline and Dolencias sinkhole. Present study was conducted in a sector 3 km in length. This

sector represents only 2 % of the entire subterranean system (Fig. 5, Grupo Espeleologico Edelweiss, 1986; Camacho et al., 2006).

Previous studies have described Ojo Guareña as an underground environment with strong rapid (daily) variations in temperature and trace gases concentration (CO_2 and ^{222}Rn). This indicates a high-energy exchange between the exterior atmosphere and the cavity (during an annual cycle cave temperatures and CO_2 concentrations ranges are 2-11^{o}C and 400-4500 ppm, respectively, Fernandez-Cortes et al., 2015a). This cave presents seasonally reversing, chimney-effect winds, which is typical of caves with multiple connections with exterior atmosphere (Mangin and Andrieux, 1988).

Ojo guareña cave system is developed by a sinking stream that inundates the most of the gallery during the rainfall periods (Fernandez-Cortes et al., 2015a). It constitutes the main water supply from exterior. The inflow rate of water via the Ojo Guareña sinking Stream ranges from 0.1 $m^3 s^{-1}$ during the dry season to 0.65 $m^3 s^{-1}$ in winter and spring (Grupo Espeleologico Edelweiss Grupo Espeleológico Edelweiss 1986). In general, chemical dissolution dominates over carbonate precipitation. The more isolated spots inside the cave, with very low energy and matter exchange, presents active speleothems, as Museo de Cera chamber (Fig. 5).

2.1.4 Rull

Rull cave is located in massive Miocene conglomerates, with considerable textural and petrophysical complexity, which were deposited on Cretaceous limestones (Pla et al., 2016 and 2017a, b). The cave consists in a single chamber with relatively small dimensions compared to the other study sites surveyed in the study (Fig. 6).

The geographical area of Rull cave is characterized by a Mediterranean or specifically Warm temperate climate with a dry and hot summer (Csa climate type, Köppen-Geiger Classification

slightly modified, AEMET-IM, 2011, Fig. 2, Table 1). Mean annual temperature in Rull cave area is around 16^{o}C and total annual precipitation is approximately 300 mm.

Rull cave environment has a high thermo-hygrometric stability throughout an annual cycle. Mean temperature inside the cavity is of 16.4 °C and the thermal amplitude is lower than 0.5 °C. The gaseous regimen in the indoor atmosphere is characterized by annual cycles with two main stages. Throughout the outgassing stage, ventilation (temperature-driven airflow) is responsible for the gaseous removal from the cavity when the cave temperature is higher than the outdoor temperature. During the warmest season, when outdoor temperature is higher than the cave temperature, the cavity suffers an isolation stage; the gaseous interchange is limited and, as consequence, the gaseous concentration increases sharply (Pla et al., 2016). This pattern is typical of caves with a downward tendency with a unique entrance located on the top (such as the Rull cave, Mangin and Andrieux, 1988). Colder and heavier air inflows in the cavity expelling the inner warmer and lighter air. Throughout an annual cycle, in Rull cave, CO_2 air concentrations normally range from 800 to 4000 ppm.

The water infiltration through dripping points is the main process of water recharge in Rull cave. There are not any evidences of water runoff along the cave passages. The cave presents low seeping rates during an annual cycle with maximum dripping during winter (Pla, 2017b). Torrential rainfalls primarily control dripping water activation. Inside the cave, there is a large quantity of speleothems (stalactites, stalagmites, flowstones etc.) with diverse mineralogy although prevailing calcite.

2.1.5 El Sidron

The karstic site of El Sidron is found in the so-called ‘‘Surco Oviedo-Infiesto’’ a strip of Mesozoic and Cenozoic sediments limited by Paleozoic relief to the north and south. The cavity is a pression tube of 600 m long, with a central stretch of 200 m oriented nearly west east. This

tube shows on its southern bank transverse galleries in a NE–SW to N–S direction, generally of a restricted nature (Fig. 7, Rosas et al., 2006).

El Sidron cave is influenced by an Oceanic or specifically Warm temperate climate, fully humid with a temperate summer (Cfb climate type of the Köppen-Geiger Classification slightly modified, AEMET-IM, 2011, Fig. 2, Table 1). Mean annual temperature is approximately 13.1 ^{o}C and annual precipitation is around 1300 mm. Own data (not published) show a stable interior temperature throughout the year around 12 ^{o}C and relatively high ventilation rate characteristic of caves with multiple connections with the surface (Mangin and Andrieux, 1988).

El Sidron cave is part of a karstic valley developed by a stream feed by external runoff and infiltration waters. It disappears in the eastern part of the valley in a sinkhole that descends to lower karstic levels (Peña et al., 2011). The main gallery of El Sidron cave is seasonally flooded and subterranean river is active throughout year with high water flow during the rainy seasons. Speleothems can be observed in the cave, mainly flowstones, though chemical dissolution dominates over carbonate precipitation.

2.1 Monitoring systems

Surface stations recorded climate parameter variability outside the caves: temperature, relative humidity and rainfall amount. The Altamira and Castañar de Ibor caves had an additional monitoring system continuously measuring and registering the temperature and humidity in the soil zone (at 5 cm depth in Altamira and at 5, 30 and 50 cm depth in Castañar de Ibor). Inner climatic conditions (temperature, relative humidity, among others) were monitored in the Altamira, Castañar de Ibor, Ojo Guareña and Rull caves jointly with the radon-222 (^{222}Rn) concentration in the underground air as a tracer of ventilation (Lario et al., 2006; Richon et al., 2011). In the El Sidron cave, the exterior and inner temperature and relative humidity of the air were also registered. Altamira, Castañar de Ibor and Rull caves monitoring

systems were fed by electric current while El Sidron and Ojo Guareña systems were battery powered.

Rainfall amount was registered in Altamira, Castañar de Ibor, Ojo Guareña and Rull caves by RG2-M pluviometers (Onset Computer Corporation, Bourne, MA, USA, resolution 0.2 mm). Air temperature and relative humidity were monitored outside Altamira and El Sidron and inside El Sidron and Ojo Guareña caves by HOBO U23 Pro v2 probes (Onset Computer Corporation, Bourne, MA, USA, accuracy ±0.2 ^{o}C and ±2.5%, respectively). The soil water volumetric content was measured in Altamira and Castañar de Ibor by ECHO EC-10 probes (Decagon Devices, Pullman, WA, U.S.A., accuracy 1-2%). Inner air temperature and relative humidity in Castañar de Ibor and Rull caves were surveyed by Rotronic probes HygroClip S3 with a Pt100 1/10 DIN thermometer and a humidity sensor (accuracy ±0.6%). The ^{222}Rn concentration of cave air was continuously registered in Altamira, Castañar de Ibor, Ojo Guareña and Rull caves using Radim 5WP monitors (GT-Analytic KG, Lambesc, France, accuracy ±0.3 (imp·Bq/h·m^{3}).

In Altamira cave, exterior soil temperature was tested by a TMC20-HD probe (Onset Computer Corporation, Bourne, MA, USA, accuracy ±0.5 ^{o}C). Inside of the cave, air temperature and humidity were surveyed by a Pt100 1/10 DIN sensor (accuracy ±0.03 ^{o}C) and a Hygroclip 1/5 DIN (Rotronic, Bassersdorf, Switzerland, accuracy ±0.8%), respectively. In Castañar de Ibor, exterior air temperature and relative humidity were tested by a S-THB Sensor (Onset Computer Corporation, Bourne, MA, USA, accuracy ±0.2 ^{o}C and ±2.5%, respectively). Exterior soil temperature was controlled by a S-TMB-M006 sensor (Onset Computer Corporation, Bourne, MA, USA, accuracy ±0.2 °C). In Ojo Guareña cave, the exterior air temperature and relative humidity were measured with a HOBO-U21 data logger (Onset Computer Corporation, Bourne, MA, USA, accuracy ±0.01 °C and ±0.03% RH). Outside of the Rull cave, a weather station with an independent data logger (HOBO U12, Onset Computer Corporation, Bourne,

MA, USA) recorded the air temperature (accuracy ±0.2 °C) and relative humidity (accuracy ±3.5%).

Further details related to the monitoring systems for the Altamira, Castañar de Ibor, Ojo Guareña and Rull caves can be found in previous articles (Fernandez-Cortes et al., 2011; Garcia-Anton et al., 2014a; Fernandez-Cortes et al., 2015a; Pla et al., 2016).

2.2 Collection and analysis of air samples

A specific sampling and analysis program was designed and implemented to obtain data on CO_2 (g) and $\delta^{13}CO_2$ inside of the caves, the soil above the caves and the exterior atmosphere in their emplacements. Field campaigns (1-2 days long) were periodically carried out for collecting air samples in a spatially-distributed network of points in the caves, the soils and the exterior. Sampling work was conducted in each single site during a complete annual cycle. Soil air was extracted using an iron tube nailed to the ground by means of a micro-diaphragm gas pump (KNF Neuberger, Freiburg, Germany) at 3.1 l/min at atmospheric pressure. Cave air and exterior air were sampled using a low-flow pump and the resulting air aliquots were saved in 1 l Tedlar bags with lock valves. The total number of samples collected at the different sites was 190, 265 and 482 for exterior, soil and cave air respectively. Bag samples were analysed no later than 48 h after sampling using a Picarro G2101-i analyser. The system uses *cavity ring-down spectroscopy (CRDS)* to identify and quantify the compounds contained in the analysed air (Crosson, 2008). The analyser measures the isotopologues of the carbon dioxide ($^{12}CO_2$ and $^{13}CO_2$) and automatically calculates the $\delta^{13}CO_2$. The device measurement precisions are 200 ppb and 10 ppb for $^{12}CO_2$ and $^{13}CO_2$, respectively. The resulting accuracy is 0.3‰ for $\delta^{13}CO_2$ after 5 minutes of analysis.

Three in-house standards with certified gas mixtures and known CO_2 concentration (7000 ppm, 400 ppm and zero-CO_2, supplied by PRAXAIR Spain in high-pressure gas cylinders for this study) were run regularly at the beginning and at the end of each day/session of analyses to verify the

proper functioning of the Picarro G2101-I analyser. Further details about the methodological procedures and quality results can be found in Fernandez-Cortes et al. (2015b). In addition, both in-house standards and air samples were also subjected to quality control by comparing the results obtained with the Picarro G2101-i analyser with duplicated bags collected, in situ (on field) and from cylinders, and subsequently analyzed independently in the greenhouse gas laboratory at Royal Holloway University of London (RHUL). CH_4 and CO_2 mole fractions of these duplicated samples were measured in the RHUL lab with a Picarro G1301 CRDS analyzer and the $\delta^{13}CO_2$ was measured in triplicate by continuous flow gas chromatography isotope ratio mass spectrometry (CF GC-IRMS) using a GV Instruments TraceGas – Isoprime system (Fisher et al., 2006). Both equipments were regularly calibrated against the NOAA (National Oceanic and Atmospheric Administration) using internal secondary standard tanks gas and a NOAA standard cylinder. The repeatability obtainable with CF GC-IRMS is 0.03 ‰ for $^{13}CO_2$ for ten consecutive analyses of a standard tank (Fisher et al., 2006).

These internal and inter-comparison procedures periodically confirmed that the performance specifications regarding CO2 analyses via our CRDS analyzer were met.

2.3 Data analysis

The $CO_2/\delta^{13}CO_2$ results of the samples analysis were studied using the Keeling approach. The Keeling plot incorporates the assumption that each data point represents a mixture of two end-member gases. The first is generally considered the background atmosphere and the second end-member is assumed to be pure CO_2 (CO_2 source) that has been added to atmospheric air to produce the composition of the observed point. The isotopic composition of source CO_2 ($\delta^{13}CO_2$) is estimated with the Keeling plot by extrapolating the straight line joining the atmospheric end-member to the data point under consideration, as far as its intersection

with the $\delta^{13}C$ axis. This method is widely used to characterize the $\delta^{13}CO_2$ of ecosystem respiration (Keeling, 1958; Keeling, 1961; Yakir and Sternberg, 2000; Pataki et al., 2003), and it has recently been used to determine the source of the high concentration of CO_2 measured in caves (Spotl et al., 2005; Mattey et al., 2010; Frisia et al., 2011).

The Keeling approach is based on a simplified two-end member model: the isotopic ratio of the CO_2 concentration in the studied air mass (a) results from the proportional mixing of the $\delta^{13}CO_2$ of a background concentration of CO_2 (b) and the $\delta^{13}CO_2$ of the CO_2 added from unknown sources:

$$[CO_2]_a \cdot \delta^{13}C_a = [CO_2]_b \cdot \delta^{13}C_b + [CO_2]_s \cdot \delta^{13}C_s \quad (1)$$

The background concentration represents the CO_2 of the clean troposphere characterized by a present-day isotopic ratio of near -8‰ (Vaughn et al., 2010; Bowling et al., 2014). The method provides the value of the source without any information about the concentration or the isotopic ratio of the background component (none of them are spatially or temporally constant variables). The isotopic $^{13}C/^{12}C$ ratio of added CO_2 is easily obtained as the intercept of the fitted line of the [$1/CO_2$, $\delta^{13}CO_2$] points resulting from the analysis of the air samples. By assuming:

$$[CO_2]_a = [CO_2]_b + [CO_2]_s \quad (2)$$

and by combining equations 1 and 2:

$$\delta^{13}C_a = [CO_2]_b \cdot (\delta^{13}C_b - \delta^{13}C_s) \cdot (1/[CO_2]_a) + \delta^{13}C_s \quad (3)$$

When more than two end-members are present in the mixture of air, then the Keeling plot will give also the $\delta^{13}C$ of the pure CO_2 (CO_2 source) that would have to be added to atmospheric air to produce the composition for the data point under consideration. This is of course only an apparent composition, and does not correspond to a real source of CO_2 if there are other

processes occurring, for example, diffusion or mixing with several pure CO_2 sources that have more than a single composition for $\delta^{13}C$.

The value obtained from equation (3) reflects a general trend in the range of the isotopic variations of the different possible sources. Therefore, the $\delta^{13}C$ of the 'pure-CO_2' end-member is always an apparent value, which must be interpreted with the help of additional hypotheses or additional information, or both.

If data point (air mixtures) all lie close to a best-fit line, the conclusion is often drawn that all the points represent mixtures between atmospheric air and a single pure-CO_2 end-member. In practice, data often scatters closely around a best-fit line and it can be attributed either to measurement and sampling errors or to composition fluctuations of the pure-CO2 end-member. When the scatter is greater, other models have to be considered (e.g., diffusion or mixing with other CO_2 sources).

In this work, the conceptual frame established for the fieldwork and data analysis is essentially based on advective and diffusive CO_2 exchange between exterior atmosphere, soil and the caves environments (according to Fig. 1). On the basis of previous work carried out in these sites (Fernandez-Cortes et al., 2009; Garcia-Anton, 2014b; Fernandez-Cortes et al., 2015; Pla et al., 2016), we assume that drip water CO_2 degassing is present but its contribution to the total CO_2 concentration of the underground environments is considered negligible compared to the transport processes in gaseous phase (i.e. advection or diffusion).

The applicability of the Keeling plot has been proven in environments where the mixing process between air masses occurs by bulk advection (Bowling and Massman, 2011; Buchmann et al., 1998; Zobitz et al., 2006). However, the assumption of the model for diffusive environments (e.g., from the air-filled porosity of soils to the open atmosphere) could lead to misinterpretation relative to the isotopic ratio of the source (Risk and Kellman, 2008; Nickerson and Risk, 2009). The diffusive process introduces an isotopic fractionation in the CO_2

input to the resulting concentration (established at -4.4‰ in stationary conditions, Craig, 1953; Cerling et al., 1991). Then, the value obtained with the model refers to the isotopic ratio of the CO_2 that enhances the concentration, which is different from the original due to the fractionation suffered during the mixing process.

3 Results

3.1 Exterior samples

The CO_2 recorded in the exterior atmosphere of the studied field sites varied over a narrow range both among sites (399.1 to 476.4 ppm; Table 2, 3) as well as temporally within sites (less than 32 ppm). The $\delta^{13}C$ of CO_2 showed a modest range among sites (-13.2 to -8.2‰) but minor temporal variations (less than 2.6‰). These values are consistent to clean atmospheric conditions slightly modified by organic activity due to the proximity of the sampling to the surface. In each field campaign, the variability in the parameters was relatively low, with maximum ranges of variation of 97.5 ppm and 3.6‰ for CO_2 and $\delta^{13}CO_2$, respectively.

3.2 Soil samples

Soil-contained CO_2 mean values ranged from 935.5 to 8116.1 ppm and the $\delta^{13}CO_2$ from -27.2 to -18.8‰ (Fig. 8, Table 2). The soil CO_2 concentration was always greater and its isotopic ratio was always lighter than those of the exterior air. In general terms, soil samples presented much greater range both spatially as well as temporally in the soil CO_2 (compared to atmosphere). Castañar de Ibor cave presented the maximum soil CO_2 concentration (9461.2 ppm in November 2011) and the greatest seasonal range (8974.9 ppm, Table 3). Highest soil $\delta^{13}CO_2$ was observed in Rull cave (-15.3‰ in July 2014), which also presented the greatest seasonal range (10.2‰, Table 3). Lower soil concentrations of CO_2 correspond to higher values of $\delta^{13}CO_2$, which in general, were observed in summer months (Fig. 8, Table 2). This set of

values is in concordance with mixed atmospheric air and soil-produced CO_2 with a $\delta^{13}CO_2$ around -27‰ (for C3-type land plants, Amundson et al., 1998).

3.3 Cave samples

All of the samples obtained presented higher concentrations of CO_2 and lower $\delta^{13}CO_2$ than those of the exterior air. Mean values of CO_2 concentration and $\delta^{13}CO_2$ for each field campaign were from 457.7 ppm to 5678 ppm and from -26.4‰ to -12.1‰ (Fig. 8, Table 2). Altamira cave presented the highest absolute CO_2 concentration (6214.7 ppm in November 2011) and the greatest seasonal range (5886.8 ppm, Table 3). Lowest absolute CO_2 concentration was observed in Ojo Guareña cave (415.02 ppm in June 2014) and the lowest annual range was observed in Rull cave (2330.4 ppm). Minimun $\delta^{13}CO_2$ was registered in Altamira cave (-26.7‰ in March 2015) and the lowest annual range was observed in Castañar de Ibor cave (4.3‰). Maximum $\delta^{13}CO_2$ was registered in Ojo Guareña cave (-8.2‰ in June 2014), which also presented the greatest seasonal range (10.2‰, Table 3). Altamira and Castañar de Ibor caves presented their minimum CO_2 concentration and maximum $\delta^{13}CO_2$ in the summer season while their winter months are characterized by higher CO_2 values and minimum $\delta^{13}CO_2$. The opposite pattern was observed in Ojo Guareña, Rull and El Sidron caves (Fig.8, Table 2).

3.4 Estimation of the $\delta^{13}C$ of the CO_2 source

Isotope and CO_2 concentration values have been used to estimate the isotopic ratio of the CO_2 source ($\delta^{13}C_s$) using the Keeling plot method (Fig. 9). The intercept values of the Keeling plot ($\delta^{13}C_s$) for the samples collected over a year at each field site were -27.7‰ (Altamira), -25.9‰ (Castañar), -26.7‰ (Ojo Guareña), -27.6‰ (Rull) and -27.5‰ (El Sidron). These values indicate a prevalence of C3 plant activity in these systems (around -27‰, Amundson et al., 1998).

Two Keeling plots were obtained for each sampling field campaign (Table 2, Fig. 10) taking into account: 1) all samples collected (in the exterior, in the soil above the cave and inside the cave)

and 2) the samples collected in the exterior air and in the soil. As a result, the temporal variations in 1) the isotopic ratio of the source for the entire system ($\delta^{13}C_s$–system) and 2) the isotopic ratio of the soil-produced CO_2 ($\delta^{13}C_s$–soil) were obtained. The $1/CO_2$ and $\delta^{13}CO_2$ values fit the Keeling model with a coefficient of determination that was higher than 0.9 (R^2>0.9). $\delta^{13}C_s$–system ranged from -24.7‰ and -29.8‰ and $\delta^{13}C_s$–soil ranged from -21.5‰ to -29.4‰ (Table 2).

The values obtained at each field site exhibited seasonal patterns. Lower values of the isotopic ratios of the sources ($\delta^{13}C_s$–system, $\delta^{13}C_s$–soil) were observed during the wetter and colder months, while a trend to heavier values was observed in the dryer and warmer months. Differences between the $\delta^{13}C_s$–system and $\delta^{13}C_s$–soil in the studied caves alternated their relative roles of heavier/lighter with a common trend towards $\delta^{13}C_s$–system < $\delta^{13}C_s$–soil during drier and warmer climatic conditions (Fig. 8).

4 Discussion

4.1 Temperature versus soil moisture control on CO_2 and $\delta^{13}CO_2$ in soil air

The CO_2 concentration and the $\delta^{13}CO_2$ of the air contained in the soil at each field site varied throughout the year (Fig. 8). It is well known that variations in soil CO_2 concentration and therefore in $\delta^{13}CO_2$ are regulated by both biotic and abiotic processes (Moyes et al., 2010; Kayler et al., 2010). The organic respiration in soil by heterotrophic and autotrophic organisms is mainly determined by soil temperature and moisture. Moreover, gas transfer processes between soil and the exterior air, which determines the soil efflux, play an important role in the soil CO_2 concentration. The increase in CO_2 production with the increase in temperature has been well demonstrated in a wide number of studies (Lloyd and Taylor, 1994; Fang and Moncrief, 2001; Risk et al., 2002). However, the cause-effect relationship between soil moisture and soil CO_2 efflux is not well defined (Fang and Moncrief, 2001; Vicca et al., 2014). Soil CO_2 productivity is directly dependent on soil moisture with a relationship particularly

marked along the annual cycle by significant responses to rain events (Xu et al., 2004). Moreover, extremely wet soil conditions decrease the gas diffusivity in the soil (Hashimoto and Komatsu, 2006; Jabro et al., 2012), which could favour an increase on the soil CO_2 concentration. The Altamira and Castañar caves have a continuous record of the volumetric water content (VWC) during the sampling periods analysed here. The $\delta^{13}CO_2$ of the samples collected at the Altamira and Castañar field sites shows a well-defined linear relationship with the soil moisture, expressed as the volumetric water content (VWC, (Fig. 8 and Fig. 11B)). Throughout the studied cycles, the lower $\delta^{13}CO_2$ corresponded to higher CO_2 concentrations in the soil, marking the lower influence of exterior air in the CO_2 contained in the soil (Fig. 11B). This relationship seems to be essentially driven by soil moisture. The increase in soil water content increases respiration rates and decreases diffusivity, which increases belowground CO_2 with an isotopic ratio that is closer to the characteristic value of organic CO_2 production (lighter values). This relationship is characteristic for each field-site, pointing to a dependence on the specific vegetation, soil properties (organic matter, microbiological activity, etc.) and physical and/or climatic features. Although soil moisture has not been monitored in Ojo Guareña, Rull and El Sidron caves, these observations are also consistent with the data collected in these sites (Fig. 8). Soil CO_2 and $\delta^{13}CO_2$ seasonal variations can be observed linked to the annual climate cycle in which high soil CO_2 and light $\delta^{13}CO_2$ values are characteristic of wetter and colder months.

Regarding the temperature control on soil CO_2 and $\delta^{13}CO_2$, heavier values are observed during the summer stages in all the studied sites (Fig. 8). This probably reflects higher rates of soil-atmosphere exchange as a consequence of lower water content in the soils.

According to the observations, connection between soil and exterior air masses and respiration rates control soil CO_2 (g) concentration and its $\delta^{13}C$. High humidity conditions during the rainy season favour production and storage of CO_2 in the soil's pore space.

4.2 Sources of variation in $\delta^{13}C$ of soil-produced CO_2

The isotopic ratio of the source to the soil ($\delta^{13}C_s$–soil) distinguishes the variations in the isotopic ratio of the soil-produced CO_2, irrespective of the influence of exterior air, according to the assumed two-end member model (i.e., the air contained in the soil is a mixture of exterior air and soil-produced CO_2). The obtained isotopic ratio of the source in the soil ($\delta^{13}C_s$–soil) for each field campaign carried out in the Altamira and Castañar de Ibor caves (Table 2) was compared with the mean values of soil moisture recorded during each field campaign (Fig. 8 and 12). The set of data pairs have a common logarithmic downward trend pointing to common processes driving the isotopic ratio of the source of CO_2 in the soil. Heavier values for the isotopic ratio of the source in the soil are characteristic of drier conditions, whereas lighter values correspond to higher soil moisture (Fig. 12).

The results reported here are consistent with many previous studies, in which a heavier isotopic source value is observed during drier and warmer seasons compared to the colder and wetter months of the year (Ekberg et al., 2007; Marron et al., 2009; Goffin et al., 2014). Other studies have related the variations in the $\delta^{13}C$ of ecosystem and soil respiration to air humidity (Ekblad and Högberg, 2001; Bowling et al., 2002; Ekblad et al., 2005). This parameter is used as an index of plant moisture stress known to influence the isotopic discrimination during photosynthesis (Farquhar et al., 1982). This effect is observed in environments with a strong seasonality in the moisture contained in the air. However, the characteristic humid climate of the Altamira field site (Table 1, Fig. 8) maintains a monthly average relative humidity above 70% during the entire year, with values above 90% most of the year (Sanchez-Moral et al., 1999; Cuezva et al., 2009). Thus, seasonal variations observed in $\delta^{13}CO_2$ of soil respiration at Altamira contrast the explanation based on moisture stress suffered by the autotrophic organisms in drier conditions.

Advection and diffusion mechanisms are responsible for soil CO_2 transport to the atmosphere and to the underground system. While advection supposes a bulk movement of air without modification of the isotopic ratio of the source for the displaced air mas (soil air into the exterior), diffusion affects the isotopic ratio of the displaced gas during the process (Nickerson and Risk, 2009). Due to the weight difference between ^{13}C and the major isotopologue of C, ^{12}C, the diffusive movement of the gas results into an enlightenment of the displaced gas regarding to its original isotopic ratio. As a result, the CO_2 of the pool source (in this case the soil) could result heavier than the produced CO_2 if diffusive transport of the gas is considerably greater than production. The isotopic fractionation by diffusion is theoretically estimated in -4.4‰ (Cerling et al., 1984) but it is known that this ratio could be rather variable (Davidson, 1995). According to this, an increase of diffusion in soil would lead to heavier $\delta^{13}CO_2$ values. This effect could be occurring in our study sites as we have observed heavier values of the CO_2 source in the soil during drier periods in which less soil humidity would induce an increase of the gas diffusivity (Jabro et al., 2012).

Figure 13A presents the measurements on soil gas at the 5 fieldworks sites as a Keeling plot, including the functions modelling either the diffusion from a gas source and the advection and mixing with atmospheric air. The grey-shaded area in Figure 13A includes the soil air affected by the mixing between background atmosphere and the apparent composition of pure CO_2 produced by microbial respiration in soil. To model the mixing of pure CO_2 with atmospheric air, a theoretical concentration of CO_2 of 20000 ppm (twice the maximum concentration measured in the soil samples, roughly 9500 ppm) and a $\delta^{13}C$ ranging -26 to -28‰ for pure CO_2 produced by microbial respiration in soils containing organic matter from C3 vegetation (according to Amundson et al., 1998) were considered. The black-solid straight lines of the mixing area are labeled as % of pure additional CO_2 remaining in the soil air.

Air contained in soil above Altamira cave (particularly during summer months) is well mixed with background atmosphere and the pure CO_2 remaining in soil samples are usually below 10%. By contrast, in poor-ventilated soils the pure CO_2 remaining is higher than 10%. The wide scatter of data in soil air from Ojo Guareña, Rull and Castañar is attributed to two processes acting in combination: 1) mixing of pure CO_2 with atmospheric air and 2) isotopic fractionation of carbon in CO_2 as the gas diffuses from the soil pore-space into some other reservoir (e.g. epikarst or open atmosphere). The curved arrows in Figure 13A show the kinetic fractionation trajectory of soil CO_2 due to its upwards diffusion to open atmosphere or epikarst, modelled by a Rayleigh-type distillation process with a fractionation coefficient of 4.4‰ (based on the theoretical mass-dependent fractionation between $^{12}CO_2$ and $^{13}CO_2$ during diffusion, according to Camarda et al., 2007). The Rayleigh equation is an exponential relation that describes the partitioning of isotopes between two reservoirs as one-reservoir decreases in size, in this case the CO_2 content in soil air. Each curve arrow starts from a soil air with a different percentage of remaining pure CO_2 produced by respiration in soil. The black-solid curve starts from a theoretical source of CO_2 (2% CO_2 and -27‰ $\delta^{13}CO_2$) and the dashed arrows from a certain percentage of pure additional CO_2 (20% and 50% remaining, respectively). As an example, the curve arrow that starts from a 20% remaining of pure CO_2 has been labelled with the fraction of CO_2 remaining after Rayleigh fractionation associated to the diffusion process. In areas with lower annual rainfall rates such as Ojo Guareña, Castañar and Rull (Table 1), most of the soil air samples fit well to these diffusion curves and, therefore, this indicates an effective diffusion of CO_2 from soil to open atmosphere or to deeper soils locations and epikarst zone. Soil air with a remaining pure CO_2 that ranges between 50% and 20% undergoes gas diffusion and the resulting air mixtures measured in soil usually have a remaining fraction of soil-derived CO_2 between 0.2 and 0.5.

According to the above discussion, the diffusive transport of the gas is likely responsible for the temporal variations observed in the isotopic ratio of the soil-produced CO_2 in the sites studied

here (Fig. 8). Reduction of soil humidity during the drier season, due to less rainfall and increase of temperatures, promotes diffusion of soil produced CO_2 to the atmosphere, deeper soil layers or the epikarst. This effect would produce an enrichment of the soil contained CO_2, which in last term causes an overestimation of the CO_2 source isotopic ratio $^{13}C/^{12}C$ (organic production). Diffusion of the gas during dry season must play a major role on the gas transport process to the atmosphere, as it is strong enough to modify the isotopic signal of organic produced CO_2.

Some cave end-members of Keeling plots have a higher $\delta^{13}C$ than their corresponded soil-produced gas, which indicate that, in these cases, there are more processes involved on CO_2-transport beside the diffusion. Consequently, the added CO_2 does not directly come from the soil. The Keeling plots for soil air show considerable non-linear scatter in some cases (Fig. 13A) and this indicates that the soil data do not correspond exactly to $\delta^{13}C$ of the CO_2 fluxes produced in the soil. CO_2 data measured in soil air is actually derived from the local diffusion in the soil. This results in a preferential loss of the light isotopic fraction with remaining CO_2 which becomes isotopically heavier (higher $\delta^{13}C$) than the CO_2 actually produced in the soil.

4.3 Ventilation versus soil CO_2 production regulating CO_2 and $\delta^{13}CO_2$ in the caves

Each cavity has a characteristic environmental variability over an annual cycle (Fig. 8). It is known that the level of ventilation is determined by geomorphology, is regulated by weather variations and is therefore different in every cave (Bourges et al., 2001). In Altamira, Castañar de Ibor, Ojo Guareña and Rull caves, correlation between radon-222 (^{222}Rn) and CO_2 monthly average values showed lineal trends marking a common influence of the ventilation of the underground environments on both gases (Fig. 14). Active ventilation shifts the cave environments towards conditions that are more similar to that of the exterior atmosphere (lower concentration of CO_2 and ^{222}Rn, and higher values of $\delta^{13}CO_2$, Fig. 9 and Fig. 14), whereas the isolation of the caves favours an increase in CO_2 and ^{222}Rn, and a decrease in $\delta^{13}CO_2$.

Lower correlation of the ^{222}Rn-CO_2 values was observed in Castañar de Ibor compared to the other sites pointing to an important influence of other-than-ventilation processes on the cave air CO_2. This cave is poorly ventilated compared to the other caves and presents a CO_2 concentration always above 2000 ppm (Table 2, Fig.8). Cave air ^{222}Rn concentration (>20000 Bq/m^3) is also much greater than the other cavities due to the high content on uranium of the rock in this site (Alvarez-Gallego et al., 2015). Differences between the parameters could be due to the distinct recharge velocities. While radon exhalation is produced at a constant rate characteristic of each rock (Cigna, 2005), CO_2 inlet to the cave is linked to variations on the CO_2 concentration of the soil and the vadose zone, which may vary throughout the year. If ventilation does not exclusively control gases concentration inside Castañar de Ibor cave, differences between the gases recharge velocities could be related to different factors controlling gases production. In the case of Castañar cave, the scatter in some of the Rn-CO_2 correlations suggests that Rn is produced at a different location from CO_2. According to the findings from our previous studies, the weathering leakage process of the bedrock favours the remobilization of radionuclides (i.e. radon source) via leaching and their later settlement into the cave environment associated to mineral phases of cave deposits (Garcia-Guinea et al., 2013).

According to previous results, the Altamira and Castañar caves undergo an isolation period during the cold and wet season and a preferential ventilation period during summer (Fig. 8, Cuezva et al., 2009; Fernandez-Cortes et al., 2011). The Ojo Guareña and Rull caves agree with preliminary studies (Fernandez-Cortes et al., 2015a; Pla et al., 2015) in which the period of major ventilation is produced during the colder months of the year (Fig. 8). The results of the samplings carried out inside El Sidron cave indicate that the colder season is the period of major connection with the exterior atmosphere (Table 2).

The goodness of fit of the Keeling plots (Fig. 9) obtained with all of the samples collected in each cavity points to the CO_2 derived from roots respiration and soil organic matter (SOM) degradation as the main source of CO_2. Though SOM degradation could occur in the vadose zone (Noronha et al., 2015; Mattey et al., 2016), the caves here studied are quite shallow (except Ojo Guareña, Table 1), which reduces probability of SOM accumulation in the epikarst.

The distribution of the points in the Keeling plots highlights the characteristics and variability (referring to CO_2 and $\delta^{13}CO_2$) of each underground environment during the studied intervals (Fig. 9). The cave samples collected at Altamira, Castañar de Ibor and Rull were more similar to the soil samples, supporting the prevalence of the soil-produced CO_2 inlet into the caves. The Ojo Guareña and El Sidron caves had more scattered distributions of the points with a general trend to values closer to the exterior air conditions, indicating an important influence of the active ventilation during the majority of the year.

Figure 13B shows that cave air compositions result from mixing between atmospheric air and a CO_2-rich component with lighter isotopic compositions that lies in the range -26 to -28 ‰. These $\delta^{13}CO_2$ values are substantially lighter in comparison with those obtained in Gibraltar caves, which lie in the range -18 to -24‰ (Mattey et al., 2016). This difference of $\delta^{13}CO_2$ values indicates that CO_2 source is not related to ground air that comes from the decay of organic material washed down into the deep soil and unsaturated zone.

The black-solid straight line of the mixing area is labeled as % of pure additional CO_2 from soil remaining in the cave air (perpendicular dotted lines). The modelling of pure CO_2 mixing with atmospheric air considers both the averaged composition of the background atmosphere of the studied sites and a theoretical (and apparent) source of pure CO_2 (2% CO_2 and $\delta^{13}CO_2$ ranging -26 to -28 ‰). Cave air is well mixed with background atmosphere in highly ventilated sites as Ojo Guareña and Sidron, so that the remaining soil-derived CO_2 is usually below 3%, with a marked seasonal variation. By contrast, in poor-ventilated caves as Castañar or, even,

Altamira cave during some periods when air renewal is hindered, the remaining soil-derived CO_2 is usually above 5%.

4.4 $\delta^{13}C$ of the source of CO_2 in the soil-underground system

The high correlation of the [$1/CO_2$, $\delta^{13}CO_2$] data pairs obtained for the samples collected in the soil, the caves and the exterior air (Fig. 9) indicates that the soil and the underground environment form a system with good communication. Similar high correlations have been described in other studies (Breecker et al., 2012). The soil-produced CO_2 displaces towards the underground air filled spaces, including voids, cracks and cavities. Therefore, the values obtained for the isotopic ratio of the system ($\delta^{13}C_s$–system) characterize the zone immediately below the surface, including soil, host rock and cave and, therefore, it indicates the likely average values of $\delta^{13}C$ of CO_2 in ground air at each site. This value would then characterize the air under the surface, which can be released to the exterior atmosphere as a result of ventilation affecting soil and epikarst.

Recent studies have demonstrated an important source of CO_2 in caves located in the air-filled pore space between soil and cave (called “ground air”). Within pore space, organic decay processes would increase the isotopic signal of soil-produced CO_2. We have tested this hypothesis by comparing our data with those obtained for St. Michaels cave (Mattey et al., 2016, Figure 13B). The isotopic ratios of the samples collected in St. Michaels are heavier than the isotopic ratios observed in our caves. This could be due to a less influence of the ground reservoir in our study sites, as our locations are significant less deeper (St. Michaels cave is located at >100m depth, Mattey et al. 2016). Moreover, the proximity of St. Michaels cave to the sea enhances the rate of water-rock interaction and would lead to more positive values of $\delta^{13}C$ of cave air.

The set of values obtained for $\delta^{13}C_s$–system at Altamira and Castañar de Ibor for each field campaign exhibited a downward logarithmic trend with soil moisture (Fig. 15). The isotopic

ratio of the source in the system had heavier values as the soil moisture decreased. The correlation of the set of points to the obtained function is, in this case, higher than that obtained with the set of values for $\delta^{13}C_s$–soil. Consequently, there could be a common control over the isotopic ratio of the source of the CO_2 contained in the soil and the CO_2 contained in the underground system. According to this, the increase of diffusion related to the reduction of soil humidity would shift the isotopic ratio of the source in the soil towards higher values due to fractionation effect during the transport process to the atmosphere. As a result, the CO_2 reservoir located in the soil would have an isotopic signal heavier during the drier season than during the rainy months of the year. Therefore, the CO_2 source for the underground system would be also affected by the seasonal enrichment of the isotopic ratio.

According to the trend obtained as a function of the soil volumetric water content in the two emplacements analysed, the isotopic ratio of the source in the systems ranged between -20.29‰ and -28.16‰ for the boundary conditions of soil moisture (Fig. 15). The boundary conditions have been taken as the accuracy of the VWC probe (0.01%) and the maximum of the soil porosities between the specific monitored sites (i.e. 48% in Altamira field site). Under lowest levels of soil volumetric water content, the underground contributes an isotopic ratio of around -20.29‰, representing the isotopic ratio of the CO_2 stored in the underground system. When soil is completely water saturated, the CO_2 stored underground is more similar than organically produced CO_2 with values around -28.16‰. The CO_2 with a characteristic light $\delta^{13}C$ stored under the surface -in the air filling space contained in the soil and the rock (including the cave)- could be released to the exterior atmosphere as a result of ventilation.

Alternatively, the range of temporal variations of $\delta^{13}C_s$–system was lower compared to that of $\delta^{13}C_s$–soil for the Altamira, Castañar de Ibor, Ojo Guareña and Rull caves (Fig.8). There appears to be a damping effect over the isotopic ratio of the soil-produced CO_2 descending towards the caves. This points to a slow transference of the gas from soil to the underground, buffering the

rapid variations in the isotopic ratio throughout deeper zones. However, the absence of a lag between the δ^{13}Cs–system and the δ^{13}Cs–soil signals could also imply that CO_2 is transported into the cave by advective mechanism.

The temporal evolution of the $\delta^{13}CO_2$ of the source presents seasonal variations due to the processes affecting the system driven by variations in weather. There was a general trend at the different field sites towards lower values of the $\delta^{13}CO_2$ of the source during wetter and colder conditions. On the contrary, heavier values were obtained in drier and warmer conditions (Fig. 8). In the sites studied here, the isotopic ratio of the source in the system ($\delta^{13}C_s$–system) was between 1 and 3‰ heavier during the summer than during the winter (Fig. 2 and Table 2). Moreover, the greatest differences between $\delta^{13}C_s$–soil and $\delta^{13}C_s$–system are observed in caves located in the zone of Mediterranean climate with higher mean temperature and lower annual precipitation rate (Castañar de Ibor, and Rull caves, Table 1). According to the results, the gas transport processes occurring and affecting the isotopic ratio of the soil-produced CO_2 seem to drive the seasonal evolution of the isotopic ratio characteristic of the CO_2 stored in the underground system ($\delta^{13}C_s$–system, Fig. 2).

5 Conclusions

The present study has shown that joint characterization of CO_2 concentration and $\delta^{13}CO_2$ from cave and soil air and exterior atmosphere is a useful and suitable method for characterizing the sources and processes involved in the CO_2 exchanges between shallow underground systems and the troposphere on an annual scale. The values obtained in the monthly and bimonthly field campaigns in several distinct caves identified seasonal patterns in the isotopic ratio of soil air and the underground atmosphere. The $\delta^{13}CO_2$ marks periods of isolation/ventilation, whereby the caves alternate their role as a reservoir or source of CO_2 on an annual scale. These data are consistent with the annual microclimatic behaviour characteristics for each

cavity and their respective locations. All of the cases confirmed that the CO_2 contained in the cave is originated as the result of the organic activity supported in the overlying soil.

Climate models predict an intensification of extreme events (Ciais et al., 2013). Previous studies have demonstrated that among them, drought has the strongest impact on terrestrial carbon cycling (Frank et al., 2015). Specifically, droughts have observed to produce a substantial reduction of the ecosystems carbon sink capability (Ciais et al., 2005, Schwalm et al., 2012), which results on positive carbon-climate feedbacks. This study shows an increase of CO_2 emissions from subsoil linked to dry periods in 5 different locations with 2 distinct climates. Therefore, the CO_2 release from vadose zone may contribute to the atmospheric CO_2 enhancement resulted from the intensive droughts expected throughout the present century because of climate change.

Acknowledgements

This research was funded by the Spanish Ministry of Economy and Competitiveness projects CGL2016-78318-C2-1R and CGL2016-78318-C2-2R AEI/FEDER/UE and its programme Torres Quevedo (PTQ 13-06296). Funding was also provided by the People Programme (Marie Curie Actions-Intra-European Fellowships, call 2013) of the European Union's Seventh Framework Programme (FP7/2007-2013) under the REA grant agreement nº 624204. We thank the cave managers for their collaboration throughout the entire investigation.

References

AEMET-IM, 2011. Iberian Climate Atlas. Air temperature and precipitation (1971-2000) in Agencia Estatal de Metereologia (España), Instituto de Metereologia (Portugal) (Eds.) http://www.aemet.es/es/conocermas/publicaciones/detalles/Atlas-climatologico

Alonso-Zarza, A.M., Martin-Perez, A., Martin-Garcia, R., Gil-Pena, I., Melendez, A., Martinez-Flores, E., Hellstrom, J., Munoz-Barco, P., 2011. Structural and host rock controls on the

distribution, morphology and mineralogy of speleothems in the Castanar Cave (Spain). Geol. Mag. 148, 211-225.

Alvarez-Gallego, M., Garcia-Anton, E., Fernandez-Cortes, A., Cuezva, S., Sanchez-Moral, S., 2015. High radon levels in subterranean environments: monitoring and technical criteria to ensure human safety (case of Castañar cave, Spain). J. Environ. Radioactiv. 145, 19-29.

Amundson, R., Stern, L., Baisden, T., Wang, Y., 1998. The isotopic composition of soil and soil-respired CO_2. Geoderma 82, 83-114.

Baldini, J.U.L., Baldini, L.M., McDermott, F., Clipson, N., 2006. Carbon dioxide sources, sinks, and spatial variability in shallow temperate zone caves: Evidence from Ballynamintra Cave, Ireland. J. Cave Karst Stud. 68, 4-11.

Berner, R.A., 2003. The long-term carbon cycle, fossil fuels and atmospheric composition. Nature 426, 323-326.

Bourges, F., Mangin, A., d'Hulst, D., 2001. Le gaz carbonique dans la dynamique de l'atmosphère des cavités karstiques : l'exemple de l'Aven d'Orgnac (Ardèche). C.R. Acad. Sci., Ser. IIa: Earth Planett. Sci. 333, 685-692.

Bowling, D., McDowell, N., Bond, B., Law, B., Ehleringer, J., 2002. 13C content of ecosystem respiration is linked to precipitation and vapor pressure deficit. Oecologia 131, 113-124.

Bowling, D.R., Massman, W.J., 2011. Persistent wind-induced enhancement of diffusive CO_2 transport in a mountain forest snowpack. J. Geophys. Res. Biogeo. 116, G04006.

Bowling, D.R., Ballantyne, A.P., Miller, J.B., Burns, S.P., Conway, T.J., Menzer, O., Stephens, B.B., Vaughn, B.H., 2014. Ecological processes dominate the 13C land disequilibrium in a Rocky Mountain subalpine forest. Global Biogeochem. Cy. 28, 352–370.

Breecker, D.O., Payne, A.E., Quade, J., Banner, J.L., Ball, C.E., Meyer, K.W., Cowan, B.D., 2012. The sources and sinks of CO_2 in caves under mixed woodland and grassland vegetation. Geochim. Cosmochim. Acta 96, 230-246.

Buchmann, N., Hinckley, T.M., Ehleringer, J.R., 1998. Carbon isotope dynamics in Abies amabilis stands in the Cascades. Can. J. Forest Res. 28, 808-819.

Camacho, A.I., Valdecasas, A.G., Rodriguez, J., Cuezva, S., Lario, J., Sanchez-Moral, S., 2006. Habitat constraints in epikarstic waters of an Iberian Peninsula cave system. Ann. Limnol. Int. J. Lim. 42, 127-140.

Camarda, M., Gregorio, S.D., Favara, R., Gurrieri S., 2007. Evaluation of carbon isotope fractionation of soil CO_2 under an advective-diffusive regimen: a tool for computing the isotopic composition of unfractionated deep source. Geochim. Cosmochim. Acta 71, 3016–3027.

Cerling, T.E., 1984. The stable isotopic composition of modern soil carbonate and its relationship to climate. Earth Pl. Sc. Lett. 71, 229-240.

Cerling, T.E., Solomon, D.K., Quade, J., Bowman, J.R., 1991. On the isotopic composition of carbon in soil carbon-dioxide. Geochim. Cosmochim. Acta 55, 3403-3405.

Chen, X., Wang, W., Luo, G., Ye, H., 2014. Can soil respiration estimate neglect the contribution of abiotic exchange? J. Arid Land 6, 129-135.

Christoforou, C.S., Salmon, L.G., Cass, G.R., 1996. Air exchange within the Buddhist cave temples at Yungang, China. Atmos. Environ. 30, 3995-4006.

Choppy, J., 1983. Phénomènes Karstiques: Dynamique de l´air. Processus Climatiques . Spéléo Club de Paris et Club Alpin Français. Paris, 84 pp.

Ciais, P., Sabine, C., Bala, G., Bopp, L., Brovkin, V., Canadell, J., Chhabra, A., DeFries, R., Galloway, J., Heimann, M., Jones, C., Le Quéré, C., Myneni, RB., Piao, S., Thornton, T., 2013. Carbon and Other Biogeochemical Cycles. In: Stocker, T.F., Qin, D., Plattner G.K., Tignor, M., Allen S.K., Boschung J., Nauels A., Xia Y., Bex, V., Midgley, P.M. (Eds). Climate change 2013: The Physical Science Basis (chapter 6), Contribution of Working Group I to the Fifth Assessment Report of the Intergovernmental Panel on Climate Change. Cambridge Univ. Press, Cambridge, pp. 465-570.

Ciais, P., Reichstein, M., Viovy, N., Granier, A., Ogee, J., Allard, V., Aubinet, M., Buchmann, N., Bernhofer, C., Carrara, A., Chevallier, F., De Noblet, N., Friend, A.D., Friedlingstein, P., Grunwald, T., Heinesch, B., Keronen, P., Knohl, A., Krinner, G., Loustau, D., Manca, G., Matteucci, G., Miglietta, F., Ourcival, J.M., Papale, D., Pilegaard, K., Rambal, S., Seufert, G., Soussana, J.F., Sanz, M.J., Schulze, E.D., Vesala, T., Valentini, R., 2005. Europe-wide reduction in primary productivity caused by the heat and drought in 2003. Nature 437, 529-533.

Cigna, A.A., 2005. Radon in caves. Int. J. Speleol. 34, 1-18.

Craig, H., 1953. The geochemistry of the stable carbon isotopes. Geochim. Cosmochim. Acta 3, 53-92.

Crosson, E.R., 2008. A cavity ring-down analyzer for measuring atmospheric levels of methane, carbon dioxide, and water vapor. Appl. Phys. B-Lasers O. 92, 403-408.

Cuezva, S., 2008. Dinámica microambiental de un medio kárstico somero (Cueva de Altamira, Cantabria): microclima, geomicrobiología y mecanismos de interacción cavidad-exterior. Ph. D. Thesis, Universidad Complutense de Madrid, Madrid, p. 320.

Cuezva, S., Sanchez-Moral, S., Saiz-Jimenez, C. and Cañaveras J.C., 2009. Microbial Communities and Associated Mineral Fabrics in Altamira Cave, Spain. Int. J. Speleol. 38 83-92.

Cuezva, S., Fernandez-Cortes, A., Benavente, D., Serrano-Ortiz, R., Kowalski, A.S., Sanchez-Moral, S., 2011. Short-term CO_2(g) exchange between a shallow karstic cavity and the external atmosphere during summer: Role of the surface soil layer. Atmos. Environ. 45, 1418-1427.

Davidson, G.R., 1995. The stable isotopic composition and measurement of carbon in soil CO_2. Geochim. Cosmochim. Acta 59, 2485-2489.

Ekberg, A., Buchmann, N., Gleixner, G., 2007. Rhizospheric influence on soil respiration and decomposition in a temperate Norway spruce stand. Soil Biol. Biochem. 39, 2103-2110.

Ekblad, A., Högberg, P., 2001. Natural abundance of ^{13}C in CO_2 respired from forest soils reveals speed of link between tree photosynthesis and root respiration. Oecologia 127, 305-308.

Ekblad, A., Boström, B., Holm, A., Comstedt, D., 2005. Forest soil respiration rate and $\delta^{13}C$ is regulated by recent above ground weather conditions. Oecologia 143, 136-142.

Faimon, J., Troppová, D., Baldík, V., Novotný, R., 2012. Air circulation and its impact on microclimatic variables in the Císařská Cave (Moravian Karst, Czech Republic). Int. J. Climatol. 32, 599-623.

Fang, C., Moncrieff, J.B., 2001. The dependence of soil CO_2 efflux on temperature. Soil Biol. Biochem., 33, 155-165.

Farquhar, G., O'Leary, M., Berry, J., 1982. On the Relationship Between Carbon Isotope Discrimination and the Intercellular Carbon Dioxide Concentration in Leaves. Funct. Plant Biol. 9, 121-137.

Fernandez-Cortes, A., Sanchez-Moral, S., Cuezva, S., Cañaveras, J.C., Abella, R., 2009. Annual and transient signatures of gas exchange and transport in the Castañar de Ibor cave (Spain). Int. J. Speleol. 38, 153-162.

Fernandez-Cortes, A., Sanchez-Moral, S., Cañaveras, J.C., Cuevas-Gonzalez, J., Cuezva, S., Andreu, J.M., 2010. Variations in seepage water geochemistry induced by natural and anthropogenic microclimatic changes: Implications for speleothem growth conditions, Geodinamica Acta. Taylor & Francis, pp. 1-13.

Fernandez-Cortes, A., Sanchez-Moral, S., Cuezva, S. Benavente, D. and Abella, R., 2011. Characterization of trace gases' fluctuations on a 'low energy' cave (Castañar de Íbor, Spain) using techniques of entropy of curves. Int. J. Climatol. 31, 127-143.

Fernandez-Cortes, A., Benavente, D., Cuezva, S., Cañaveras, J.C., Alvarez-Gallego, M., Garcia-Anton, E., Soler, V., Sanchez-Moral, S., 2013. Effect of water vapour condensation on the radon content in subsurface air in a hypogeal inactive-volcanic environment in Galdar cave, Spain. Atmos. Environ. 75, 15-23.

Fernandez-Cortes, A., Cuezva, S., Garcia-Anton. E., Alvarez-Gallego., M., Pla, C., Benavente, D., Cañaveras, J.C., Calaforra, J.M., Mattey, D.P., Sanchez-Moral, S., 2015a. Changes in the storage and sink of carbon dioxide in subsurface atmospheres controlled by climate-driven processes: the case of the Ojo Guareña karst system. Environ. Earth Sci 74, 7715-7730.

Fernandez-Cortes, A., Cuezva, S., Alvarez-Gallego, M., Garcia-Anton, E., Pla, C., Benavente, D., Jurado, V., Saiz-Jimenez, C., Sanchez-Moral, S., 2015b. Subterranean atmospheres may act as daily methane sinks. Nature Commun. 6, 7003.

Fisher, R., Lowry, D., Wilkin, O., Sriskantharajah, S., Nisbet, E. G., 2006. High-precision, automated stable isotope analysis of atmospheric methane and carbon dioxide using continuous-flow isotope-ratio mass spectrometry, Rapid Commun. Mass Sp., 20, 200-208.

Frank, D.A., Reichstein, M., Bahn, M., Thonicke, K., Frank, D., Mahecha, M.D., Smith, P., Van der Velde, M., Vicca, S., Babst, F., Beer, C., Buchmann, N., Canadell, J.G., Ciais, P., Cramer, W., Ibrom, A., Miglietta, F., Poulter, B., Rammig, A., Seneviratne, S.I., Walz, A., Wattenbach, M.,

Zavala, M.A., Zscheischler, J., 2015. Effects of climate extremes on the terrestrial carbon cycle: concepts, processes and potential future impacts. Glob. Change Biol. 21, 2861-2880.

Frisia, S., Fairchild, I.J., Fohlmeister, J., Miorandi, R., Spoetl, C., Borsato, A., 2011. Carbon mass-balance modelling and carbon isotope exchange processes in dynamic caves. Geochim. Cosmochim. Acta 75, 380-400.

Garcia-Anton, E., Cuezva, S., Fernandez-Cortes, A., Benavente, D., Sanchez-Moral, S., 2014b. Main drivers of diffusive and advective processes of CO_2-gas exchange between a shallow vadose zone and the atmosphere. Int. J. Greenh. Gas Con. 21, 113-129.

Garcia-Anton, E., 2014b. Aplicación de la señal isotópica $\delta^{13}CO_2$ para la caracterización de mecanismos de transporte de CO_2-gas entre atmósfera y subsuelo en sistemas kársticos someros (Cueva de Altamira, Cantabria). University of Alicante, Alicante, p. 170.

Garcia-Guinea, J., Fernandez-Cortes, A., Alvarez-Gallego, M., Garcia-Antón, E., Casas-Ruiz, M., Blázquez-Pérez, D., Teijón, O., Cuezva, S., Correcher, V., Sanchez-Moral, S., 2013. Leaching of uranyl–silica complexes from the host metapelite rock favoring high radon activity of subsoil air: case of Castañar cave (Spain). J. Radioanal. Nucl. Chem. 298, 1567-1585.

Genty, D., 2008. Palaeoclimate research in Villars Cave (Dordogne, SW-France). Int. J. Speleol. 37, 3.

Gilfillan, S.M., Lollar, B.S., Holland, G., Blagburn, D., Stevens, S., Schoell, M., Cassidy, M., Ding, Z., Zhou, Z., Lacrampe-Couloume, G., 2009. Solubility trapping in formation water as dominant CO_2 sink in natural gas fields. Nature 458, 614-618.

Goffin, S., Aubinet, M., Maier, M., Plain, C., Schack-Kirchner, H., Longdoz, B., 2014. Characterization of the soil CO_2 production and its carbon isotope composition in forest soil layers using the flux-gradient approach. Agr. Forest Meteorol. 188, 45-57.

Grupo Espeleológico Edelweiss (1986) Complejo kárstico de Ojo Guareña. In: Diputación Provincial de Burgos (Ed) Kaite, vol 4-5. Diputación Provincial de Burgos, Burgos, Spain.

Hamerlynck, E.P., Scott, R.L., Sánchez-Cañete, E.P., Barron-Gafford, G.A., 2013. Nocturnal soil CO_2 uptake and its relationship to subsurface soil and ecosystem carbon fluxes in a Chihuahuan Desert shrubland. J. Geophys. Res. Biogeo. 118, 2013JG002495.

Hashimoto, S., Komatsu, H., 2006. Relationships between soil CO_2 concentration and CO_2 production, temperature, water content, and gas diffusivity: implications for field studies through sensitivity analyses. J. For. Res. 11, 41-50.

Hemming, D., Yakir, D., Ambus, P., Aurela, M., Besson, C., Black, K., Buchmann, N., Burlett, R., Cescatti, A., Clement, R., Gross, P., Granier, A., Grünwald, T., Havrankova, K., Janous, D., Janssens, I.A., Knohl, A., Östner, B.K., Kowalski, A., Laurila, T., Mata, C., Marcolla, B., Matteucci, G., Moncrieff, J., Moors, E.J., Osborne, B., Pereira, J.S., Pihlatie, M., Pilegaard, K., Ponti, F., Rosova, Z., Rossi, F., Scartazza, A., Vesala, T., 2005. Pan-European $\delta^{13}C$ values of air and organic matter from forest ecosystems. Glob. Change Biol. 11, 1065-1093.

Jabro, J.D., Sainju, U.M., Stevens, W.B., Evans, R.G., 2012. Estimation of CO_2 diffusion coefficient at 0-10 cm depth in undisturbed and tilled soils. Arch. Agron. Soil Sci. 58, 1-9.

James, E.W., Banner, J.L., Hardt, B., 2015. A global model for cave ventilation and seasonal bias in speleothem paleoclimate records. Geochem. Geophys. Geosy. 16, 1044-1051.

Jassal, R.S., Black, T.A., Cai, T., Morgenstern, K., Li, Z., Gaumont-Guay, D., Nesic, Z., 2007. Components of ecosystem respiration and an estimate of net primary productivity of an intermediate-aged Douglas-fir stand. Agr. Forest Meteorol. 144, 44-57.

Kayler, Z.E., Ganio, L., Hauck, M., Pypker, T.G., Sulzman, E.W., Mix, A.C., Bond, B.J., 2010. Bias and uncertainty of delta(CO_2)-C-13 isotopic mixing models. Oecologia 163, 227-234.

Keeling, C.D., 1958. The concentration and isotopic abundances of atmospheric carbon dioxide in rural areas. Geochim. Cosmochim. Acta 13, 322-334.

Keeling, C.D., 1961. The concentration and isotopic abundances of carbon dioxide in rural and marine air. Geochim. Cosmochim. Acta 24, 277-298.

Kowalski, A.S., Serrano-Ortiz, P., Janssens, I.A., Sánchez-Moral, S., Cuezva, S., Domingo, F., Were, A., Alados-Arboledas, L., 2008. Can flux tower research neglect geochemical CO_2 exchange? Agr. Forest Meteorol. 148, 1045-1054.

Lalueza-Fox, C., Rosas, A., Estalrrich, A., Gigli, E., Campos, P.F., Garcia-Tabernero, A., Garcia-Vargas, S., Sanchez-Quinto, F., Ramirez, O., Civit, S., Bastir, M., Huguet, R., Santamaria, D., Gilbert, M.T.P., Willerslev, E., de la Rasilla, M., 2011. Genetic evidence for patrilocal mating behavior among Neandertal groups. P. Natl. Acad. Sci. U.S.A. 108, 250-253.

Lario, J., Sanchez-Moral, S., Cuezva, S., Taborda, M., Soler, V., 2006. High Rn-222 levels in a show cave (Castanar de Ibor, Spain): Proposal and application of management measures to minimize the effects on guides and visitors. Atmos. Environ. 40, 7395-7400.

Liu, Z., Zhao, J., 2000. Contribution of carbonate rock weathering to the atmospheric CO_2 sink. Environ. Geol. 39, 1053-1058.

Lloyd, J., Taylor, J.A., 1994. On the temperature-dependence of soil respiration. Funct. Ecol. 8, 315-323.

Mangin, A., Andrieux, C., 1988. Infiltration et environnement souterrain, le rôle de l'eau sur les paramètres climatiques. Actes des journées Félix Trombe T1, Mémoires du Spéléo-Club de Paris 14, 78-95.

Marron, N., Plain, C., Longdoz, B., Epron, D., 2009. Seasonal and daily time course of the ^{13}C composition in soil CO_2 efflux recorded with a tunable diode laser spectrophotometer (TDLS). Plant Soil 318, 137-151.

Maseyk, K., Wingate, L., Seibt, U., Ghashghaie, J., Bathellier, C., Almeida, P., de Vale, R.L., Pereira, J.S., Yakir, D., Mencuccini, M., 2009. Biotic and abiotic factors affecting the delta C-13 of soil respired CO_2 in a Mediterranean oak woodland. Isot. Environ. Healt. S. 45, 343-359.

Mattey, D.P., Fairchild, I.J., Atkinson, T.C., Latin, J.-P., Ainsworth, M., Durell, R., 2010. Seasonal microclimate control of calcite fabrics, stable isotopes and trace elements in modern speleothem from St Michaels Cave, Gibraltar. Geol. Soc. Spec. Publ. 336, 323-344.

Mattey, D.P., Atkinson, T.C., Barker, J.A., Fisher, R., Latin, J.P., Durrell, R., Ainsworth, M., 2016. Carbon dioxide, ground air and carbon cycling in Gibraltar karst. Geochim. Cosmochim. Acta 184, 88-113.

Morner, N.A., Etiope, G., 2002. Carbon degassing from the lithosphere. Global Planet. Change 33, 185-203.

Moyes, A.B., Gaines, S.J., Siegwolf, R.T.W., Bowling, D.R., 2010. Diffusive fractionation complicates isotopic partitioning of autotrophic and heterotrophic sources of soil respiration. Plant Cell Environ. 33, 1804-1819.

Nickerson, N., Risk, D., 2009. Physical controls on the isotopic composition of soil-respired CO_2. J. Geophys. Res. Biogeo. 114, G01013.

Noronha, A.L., Johnson, K.R., Southon, J.R., Hu, C., Ruan, J., McCabe-Glynn, S., 2015. Radiocarbon evidence for decomposition of aged organic matter in the vadose zone as the main source of speleothem carbon. Quaternary Sci. Rev. 127, 37-47.

Pataki, D.E., Ehleringer, J.R., Flanagan, L.B., Yakir, D., Bowling, D.R., Still, C.J., Buchmann, N., Kaplan, J.O., Berry, J.A., 2003. The application and interpretation of Keeling plots in terrestrial carbon cycle research. Global Biogeochem. Cy. 17, 1022.

Peña, J.A., 2011. Descripción física del complejo cárstico y sus conexiones exteriores, in: de la Rasilla, M., Rosas, A., Cañaveras, J.C., Lalueza-Fox, C. (Eds.), La cueva de El Sidrón (Borines, Piloña, Asturias). Investigación interdisciplinar de un grupo neandertal. Conserjeria de Cultura y Turismo. Gobierno del Principado de Asturias, pp. 21-26.

Pla, C., Cuezva, S., Garcia-Anton, E., Fernandez-Cortes, A., Cañaveras, J.C., Sanchez-Moral, S., Benavente, D., 2016. Changes in the CO_2 dynamics in near-surface cavities under a future warming scenario: Factors and evidence from the field and experimental findings. Sci. Total Environ., 565, 1151-1164.

Pla, C., Cuezva, S., Martinez-Martinez, J., Fernandez-Cortes, A., Garcia-Anton, E., Fusi, N., Crosta, G.B., Cuevas-Gonzalez, J., Cañaveras, J.C., Sanchez-Moral, S., Benavente, D., 2017a. Role of soil pore structure in water infiltration and CO_2 exchange between the atmosphere and underground air in the vadose zone: A combined laboratory and field approach. Catena 149(1), 402-416.

Pla, C., 2017b. Modelización del transporte difusivo de gases en el conjunto suelo-roca. Aplicación al análisis e interpretación de datos microclimáticos en sistemas kársticos someros. Ph. D. Thesis, Universidad de Alicante, p. 217.

Richon, P., Perrier, F., Koirala, B.P., Girault, F., Bhattarai, M., Sapkota, S.N., 2011. Temporal signatures of advective versus diffusive radon transport at a geothermal zone in Central Nepal. J. Environ. Radioactiv. 102, 88-102.

Risk, D., Kellman, L., Beltrami, H., 2002. Carbon dioxide in soil profiles: Production and temperature dependence. Geophys. Res. Lett. 29, 11-11-11-14.

Risk, D., Kellman, L., 2008. Isotopic fractionation in non-equilibrium diffusive environments. Geophys. Res. Lett. 35, L02403.

Roland, M., Serrano-Ortiz, P., Kowalski, A.S., Goddéris, Y., Sánchez-Cañete, E.P., Ciais, P., Domingo, F., Cuezva, S., Sanchez-Moral, S., Longdoz, B., Yakir, D., Van Grieken, R., Schott, J., Cardell, C., Janssens, I.A., 2013. Atmospheric turbulence triggers pronounced diel pattern in karst carbonate geochemistry. Biogeo. 10, 5009-5017.

Rosas, A., Martínez-Maza, C., Bastir, M., García-Tabernero, A., Lalueza-Fox, C., Huguet, R., Ortiz, J.E., Julià, R., Soler, V., De Torres, T., Martínez, E., Cañaveras, J.C., Sánchez-Moral, S., Cuezva, S., Lario, J., Santamaría, D., De La Rasilla, M., Fortea, J., 2006. Paleobiology and comparative morphology of a late Neandertal sample from El Sidrón, Asturias, Spain. P. Natl. Acad. Sci. U.S.A. 103, 19266-19271.

Ryan, M.G., Law, B.E., 2005. Interpreting, measuring, and modeling soil respiration. Biogeochemistry 73, 3-27.

Sanchez-Cañete, E.P., Serrano-Ortiz, P., Kowalski, A.S., Oyonarte, C., Domingo, F., 2011. Subterranean CO_2 ventilation and its role in the net ecosystem carbon balance of a karstic shrubland. Geophys. Res. Lett. 38, L09802.

Sanchez-Cañete, E.P., Serrano-Ortiz, P., Domingo, F., Kowalski, A.S., 2013. Cave ventilation is influenced by variations in the CO_2-dependent virtual temperature. Int. J. Speleol. 42, 1-8.

Sanchez-Moral, S., Soler, V., Canaveras, J.C., Sanz-Rubio, E., Van Grieken, R., Gysels, K., 1999. Inorganic deterioration affecting the Altamira Cave, N Spain: quantitative approach to wall-corrosion (solutional etching) processes induced by visitors. Sci. Total Environ. 243/244, 67-84.

Serrano-Ortiz, P., Roland, M., Sanchez-Moral, S., Janssens, I.A., Domingo, F., Godderis, Y., Kowalski, A.S., 2010. Hidden, abiotic CO_2 flows and gaseous reservoirs in the terrestrial carbon cycle: Review and perspectives Agr. Forest Meteorol. 151, 529-529.

Schwalm, C.R., Williams, C.A., Schaefer, K., Baldocchi, D., Black, T.A., Goldstein, A.H., Law, B.E., Oechel, W.C., Paw U, K.T., Scott, R.L., 2012. Reduction in carbon uptake during turn of the century drought in western North America. Nature Geosci. 5, 551-556.

Shanhun, F.L., Almond, P.C., Clough, T.J., Smith, C.M.S., 2012. Abiotic processes dominate CO_2 fluxes in Antarctic soils. Soil Biol. Biochem. 53, 99-111.

Spotl, C., Fairchild, I.J., Tooth, A.F., 2005. Cave air control on dripwater geochemistry, Obir Caves (Austria): Implications for speleothem deposition in dynamically ventilated caves. Geochim. Cosmochim. Acta 69, 2451-2468.

Vaughn, B., Evans, C., White, J.C., Still, C., Masarie, K., Turnbull, J., 2010. Global Network Measurements of Atmospheric Trace Gas Isotopes, in: West, J.B., Bowen, G.J., Dawson, T.E., Tu, K.P. (Eds.), Isoscapes: Understanding Movement, Pattern, and Process on Earth Through Isotope Mapping. Springer Netherlands, pp. 3-31.

Vicca, S., Bahn, M., Estiarte, M., van Loon, E., Vargas, R., Alberti, G., Ambus, P., Arain, M., Beier, C., Bentley, L., 2014. Can current moisture responses predict soil CO_2 efflux under altered precipitation regimes? A synthesis of manipulation experiments. Biogeosciences Discuss. 11, 2991-3013.

Wang, W., Chen, X., Luo, G., Li, L., 2014. Modeling the contribution of abiotic exchange to CO_2 flux in alkaline soils of arid areas. J. Arid Land 6, 27-36.

Xu, L., Baldocchi, D.D., Tang, J., 2004. How soil moisture, rain pulses, and growth alter the response of ecosystem respiration to temperature. Global Biogeochem. Cy. 18, GB4002.

Yakir, D., Sternberg, L.D.L., 2000. The use of stable isotopes to study ecosystem gas exchange. Oecologia 123, 297-311.

Zobitz, J.M., Keener, J.P., Schnyder, H., Bowling, D.R., 2006. Sensitivity analysis and quantification of uncertainty for isotopic mixing relationships in carbon cycle research. Agr. Forest Meteorol. 136, 56-75.

Figure captions

Figure 1: Diagram illustrating the main pathways of CO_2(g)-exchange between atmosphere, soil and the cave and major transport mechanisms between them (simplified from Mattey et al., 2016). The more complex set of processes related to vadose groundwater as vehicle of CO_2 transport to cave atmosphere (i.e. the formation of carbonic acid in soil and epikarst zone, dissolution of bedrock and degassing of drip water), has been simplified in a singled process named as "Infiltrating water". In addition, the term "Soil-derived CO_2" includes all CO_2 originally generated within soil (roots respiration and soil organic matter degradation) and the subsequent process as direct gas diffusion mainly from deeper soil layer or previously accumulated in the fissures, fractures and pore-spaces of rock in the vadose zone and, additionally, the CO_2 derived from microbial oxidation of down-washed organic matter.

Figure 2: Geographic and climatic locations of the studied caves. Climatic classification follows the Köppen-Geiger method with slight modifications (adapted from AEMET-IM, 2008). Letters B, C, D and E refers to Arid, Temperate, Continental and Polar climates. Study sites are located at temperate humid (Cfb) and temperate dry (Csa) climates also named Oceanic and Mediterranean respectively.

Figure 3: A) Plan view of Altamira cave, B) Cross section of the cave.

Figure 4: A) Plan view of Castañar cave with 5 cross sections, B) Galleries distributions in a SE-NW topography section following the maximum gradient line.

Figure 5: A) Map of the cave sectors where the study has been carried out. B) Detailed cross-sections of the cave galleries in relation to surface geomorphology and the main entrances to the subterranean system (solid black line represents the studied galleries; the ends of these galleries continue with the rest of the subterranean system, which is not drawn; the dotted lines show the locations of other cave levels).

Figure 6: A) Plan view of Rull cave, B) Cross section of the cave.

Figure 7: A) Map of the El Sidron cave system, B) Cross section of the cave.

Figure 8: Annual cycles of the main parameters registered in the Altamira, Castañar, Ojo Guareña and Rull caves. (A) monthly average temperature (circles) and total monthly rainfall (bars). (B) monthly average relative humidity in the air (triangles) and volumetric water content in the soil at 5 cm depth (circles). (C) monthly average radon concentration contained in the inner parts of the cave (squares). (D) mean values of CO_2 (squares) and $\delta^{13}CO_2$ (diamonds) for each field campaign in the cave atmosphere. (E) mean values of CO_2 (hexagons) and $\delta^{13}CO_2$ (diamonds) for each field campaign in the soil air.(F) isotopic signal $\delta^{13}C$ of the source of CO_2 for the soil ($\delta^{13}C_s$–soil, triangles) and the entire system ($\delta^{13}C_s$–system, squares) estimated using the Keeling plot model (see text). Shaded area represents the warmer months of the represented annual cycles.

Figure 9: Keeling plots of the total amount of samples collected in the soil (circles), cave (diamonds) and exterior air (squares) at each cave site.

Figure 10: Keeling plots of the samples collected in different field campaigns at the Castañar de Ibor, Ojo Guareña, Rull and El Sidron caves. Different values of the intercept were obtained for the air contained in the soil ($\delta^{13}C_s$-soil) and the entire system ($\delta^{13}C_s$-system, see text).

Figure 11: (A) Relationship between the average values $\delta^{13}CO_2$ and VWC at 5 cm depth (volumetric water content) and (B) the average values $\delta^{13}CO_2$ and CO_2 during each field campaign in the soil at Altamira (squares) and Castañar de Ibor (diamonds).

Figure 12: Relationship between the average values of $\delta^{13}C_s$-soil (isotopic ratio of the source of soil-contained CO_2 calculated from Keeling plot, see Fig. 10) and VWC (volumetric water content) at 5 cm depth at Altamira (squares) and Castañar de Ibor (diamonds).

Figure 13: Keeling plot of $1/CO_2$ versus $\delta\ ^{13}CO_2$ soil air (A) and cave air (B) for all samples collected in the 5 field sites. The dotted crosshairs correspond to the averaged composition of the 5 local atmospheres in this study. Solid squares: samples of background atmosphere, solid circles: soil air samples, and open rectangles: cave air samples. Each colour code corresponds to a single studied cave. Panel B: data points can be envisaged as representing mixtures (cave air) of average atmospheric air with a CO_2-rich component derived from soil. The keeling plots for each cave site are plotted by coloured dashed lines, according to results from Fig.9. The thicker and continuous black line corresponds to the modelled mixing process between both components (see text for further details) and the perpendicular dotted lines are contours of equal mixing ratios labelled as % of remaining (soil-derived) CO_2 in the cave air. Data for New St. Michaels cave air (Mattey et al., 2016) is also plotted for comparison (grey crosses) and interpreted as a mix of atmosphere and ground air (grey shaded area and black straight line). See text for a detailed description of the modelled processes and further discussion.

Figure 14: Linear correlation between the monthly average values of cave air ^{222}Rn and CO_2 concentrations in Altamira, Castañar de Ibor, Ojo Guareña and Rull caves during the respective sampling periods.

Figure 15: Relationship between $\delta^{13}C_s$-system (isotopic ratio of the source of system CO_2 calculated from the Keeling plot, see Fig. 10) and VWC at 5 cm depth during each field campaign in the soil at Altamira (squares) and Castañar de Ibor (diamonds).

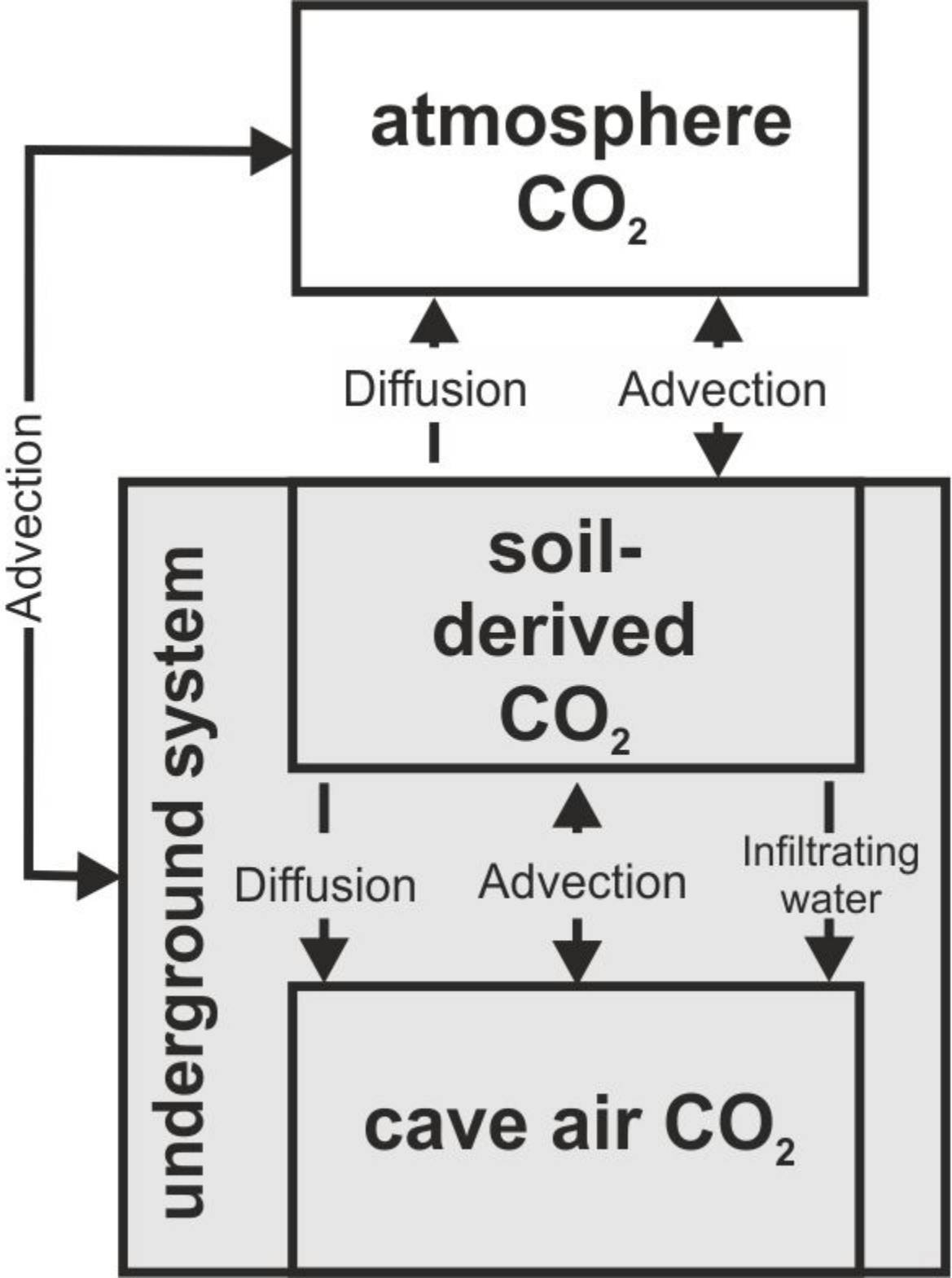
atmosphere
CO_2
Diffusion
Advection
Advection
underground system
soil-
derived
CO_2
Diffusion
Advection
Infiltrating
water
cave air CO_2

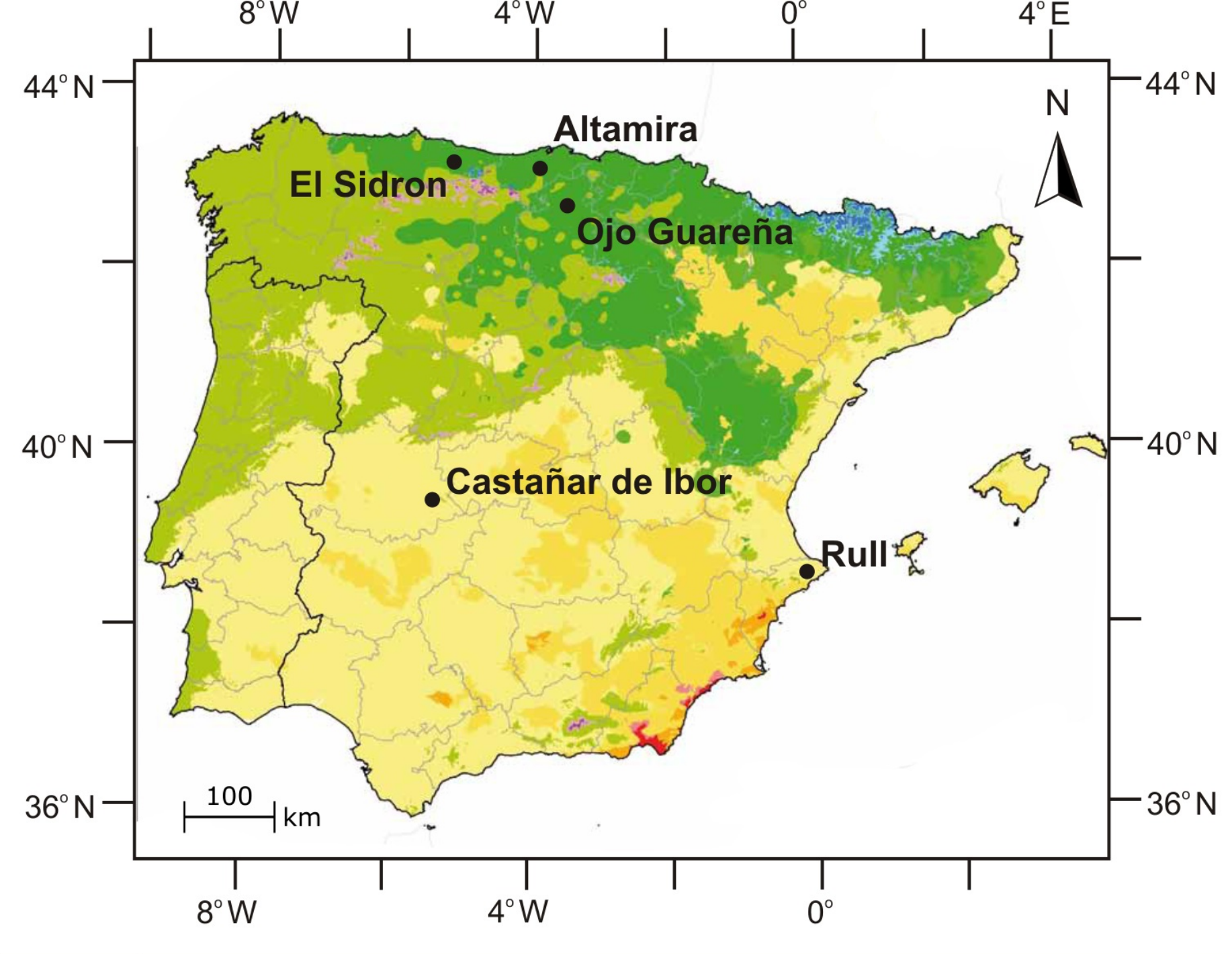

LEGEND

- BWh: hot desert
- BWh: cold desert
- BSh: hot steepe
- BSk: cold steepe
- Csa: temperate with dry and hot summer
- Csb: temperate with dry and temperate summer
- Cfa: temperate without dry season and hot summer
- Cfb: temperate without dry season and temperate summer
- Dsb: cold with dry and temperate summer
- Dsc: cold with dry and fresh summer
- Dfb: cold without dry season and temperate summer
- Dfc: cold with a dry season and fresh summer
- ET: tundra

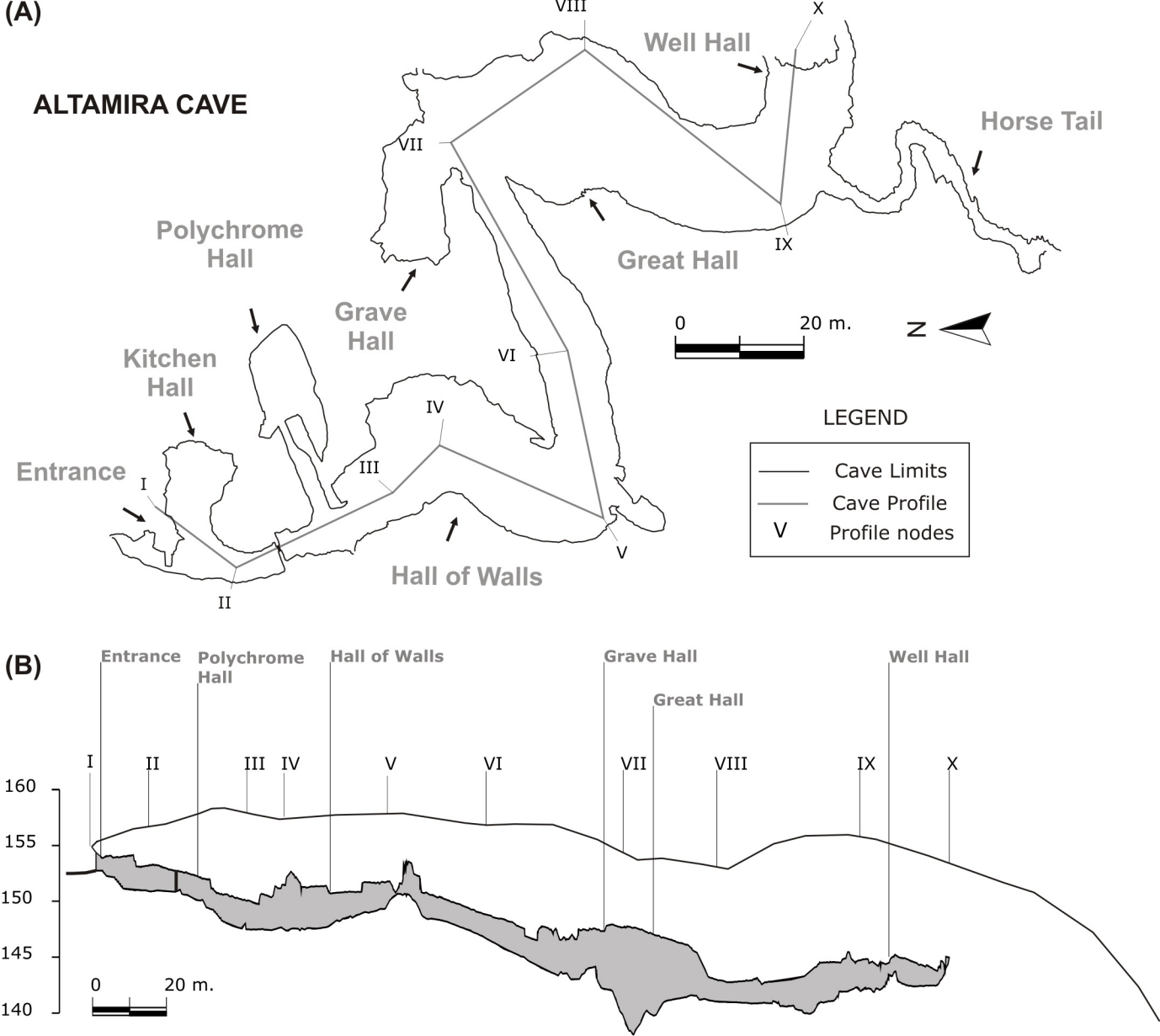
(A)
ALTAMIRA CAVE
VIII
X
Well Hall
Horse Tail
VII
Polychrome Hall
IX
Great Hall
Grave Hall
0
20 m.
N
Kitchen Hall
VI
IV
LEGEND
Cave Limits
Cave Profile
V
Profile nodes
Entrance
I
III
V
Hall of Walls
II
(B)
Entrance
Polychrome Hall
Hall of Walls
Grave Hall
Great Hall
Well Hall
I
II
III
IV
V
VI
VII
VIII
IX
X
160
155
150
145
140
0
20 m.

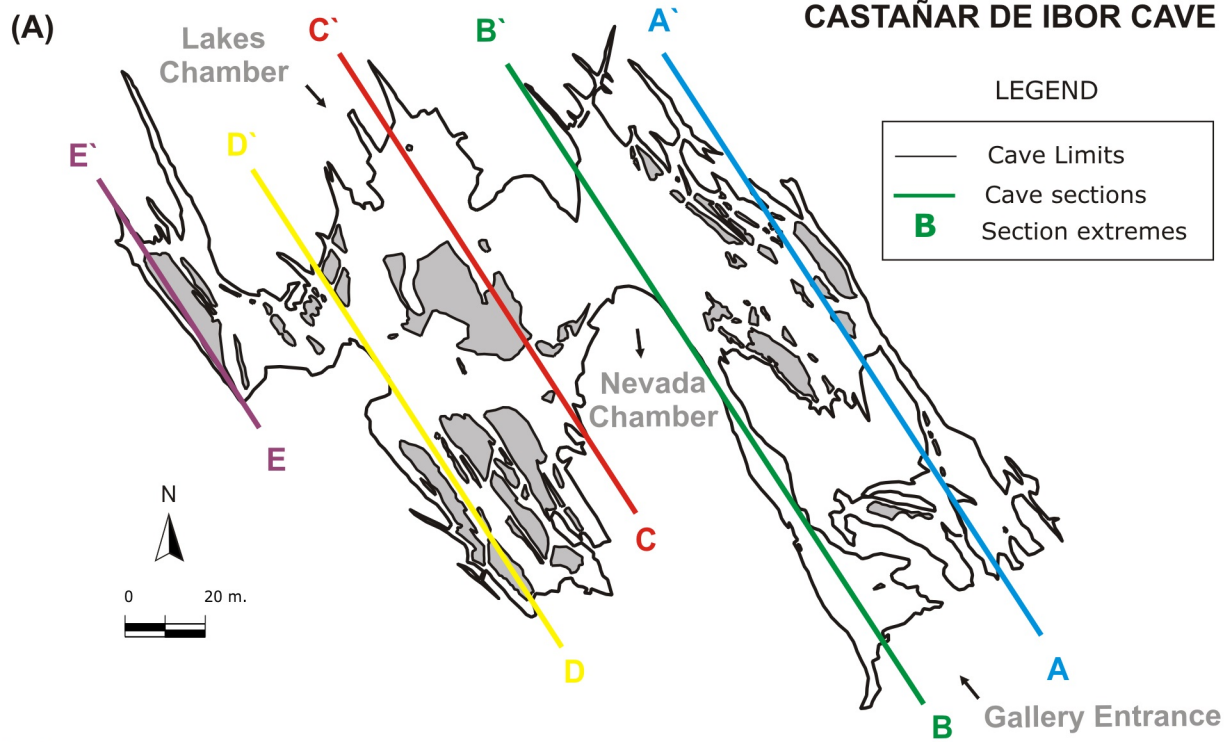
(A)
CASTAÑAR DE IBOR CAVE
LEGEND
Cave Limits
Cave sections
B
Section extremes
Lakes Chamber
Nevada Chamber
Gallery Entrance
A`
B`
C`
D`
E`
A
B
C
D
E
N
0
20 m.

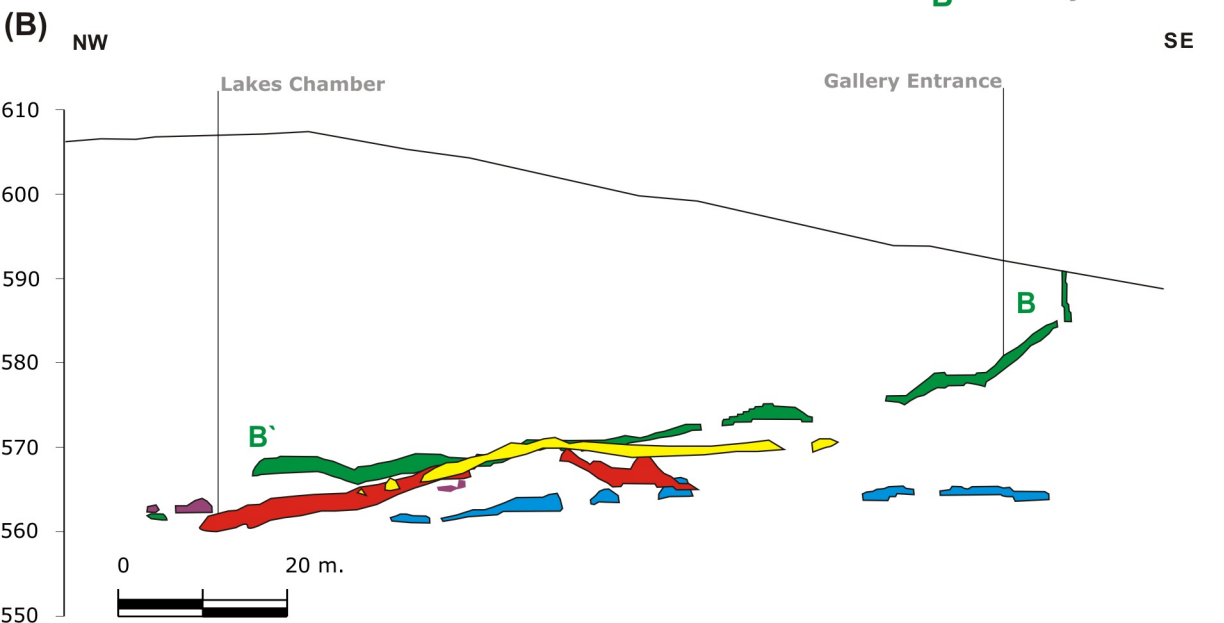
(B)
NW
SE
Lakes Chamber
Gallery Entrance
610
600
590
580
570
560
550
B
B`
0
20 m.

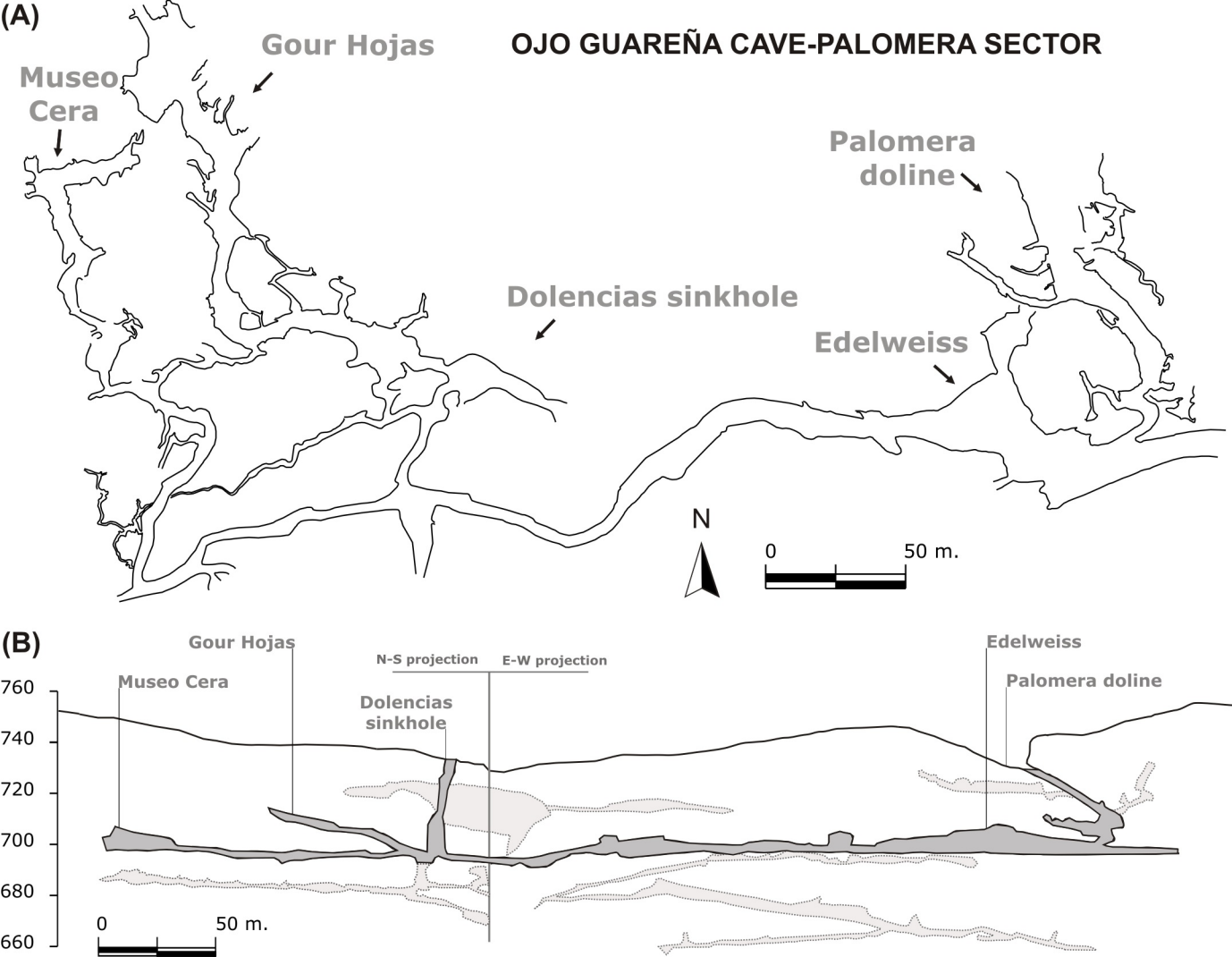
(A)
OJO GUAREÑA CAVE-PALOMERA SECTOR
Museo Cera
Gour Hojas
Palomera doline
Dolencias sinkhole
Edelweiss
N
0
50 m.
(B)
Gour Hojas
Museo Cera
N-S projection
E-W projection
Dolencias sinkhole
Edelweiss
Palomera doline
760
740
720
700
680
660
0
50 m.

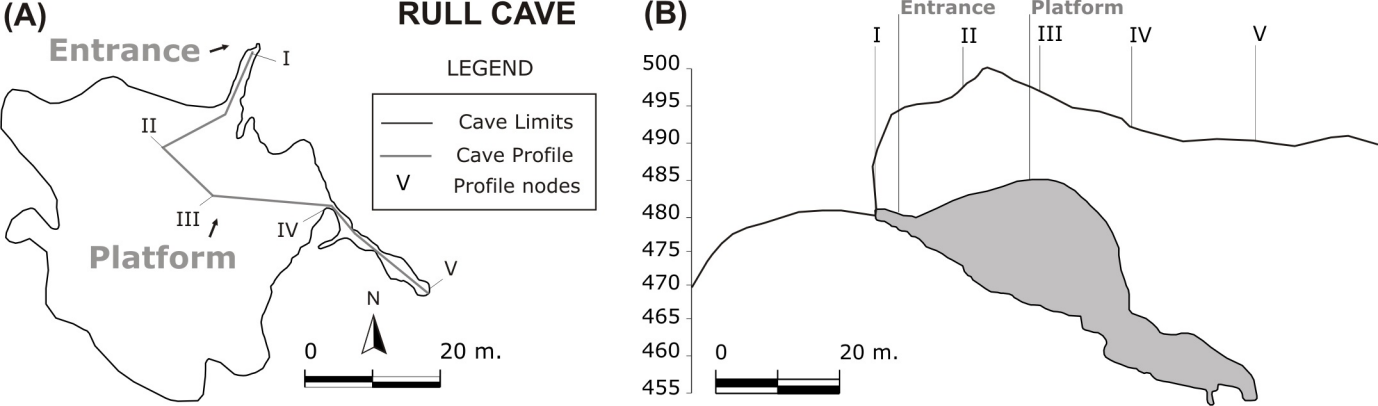
(A)
RULL CAVE
Entrance
I
II
III
IV
V
Platform
LEGEND
Cave Limits
Cave Profile
Profile nodes
N
0
20 m.
(B)
Entrance
Platform
I
II
III
IV
V
500
495
490
485
480
475
470
465
460
455
0
20 m.

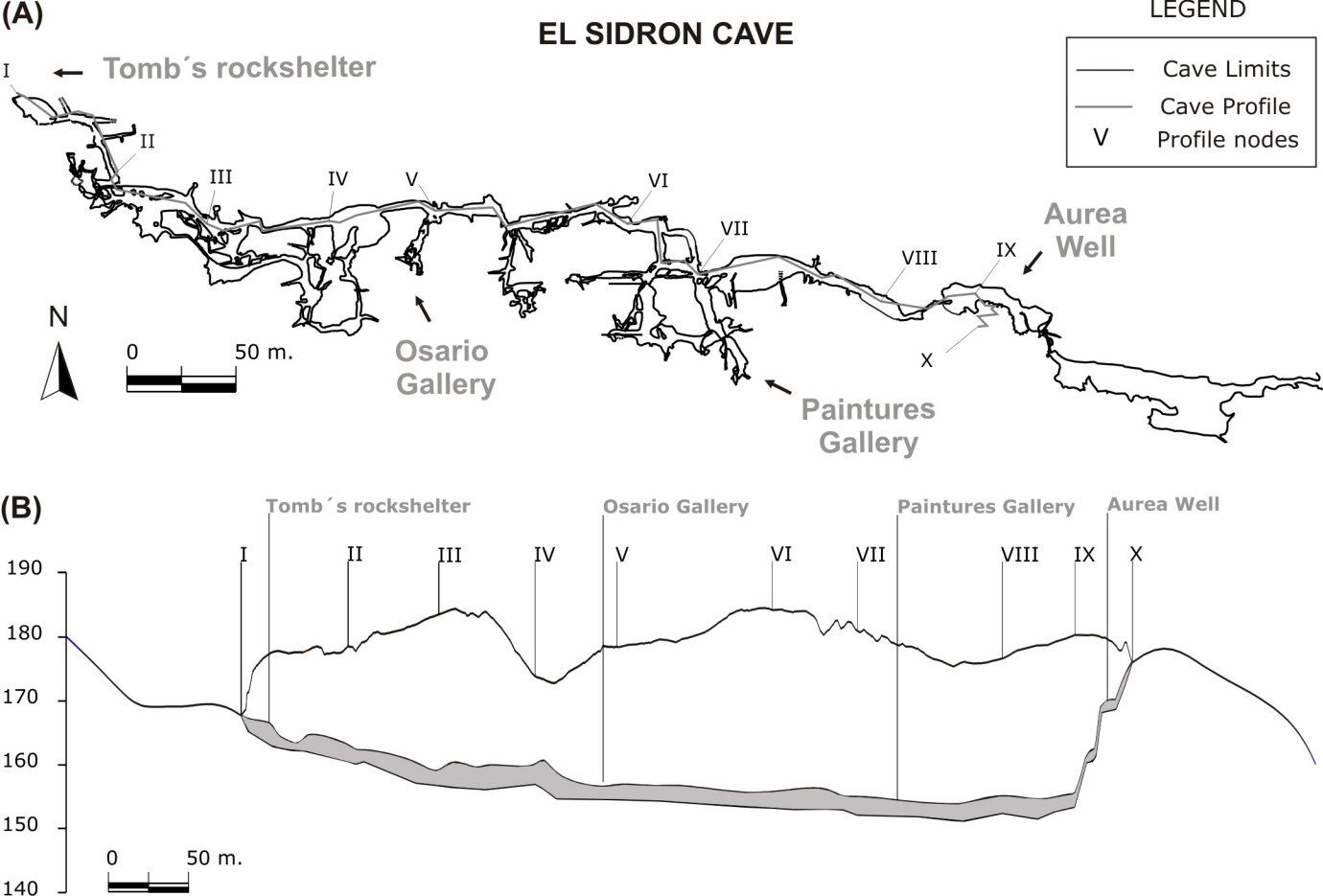
(A)
EL SIDRON CAVE
LEGEND
Cave Limits
Cave Profile
V Profile nodes
Tomb´s rockshelter
I
II
III
IV
V
VI
VII
VIII
IX
X
Aurea Well
Osario Gallery
Paintures Gallery
N
0
50 m.
(B)
Tomb´s rockshelter
Osario Gallery
Paintures Gallery
Aurea Well
190
180
170
160
150
140
0
50 m.

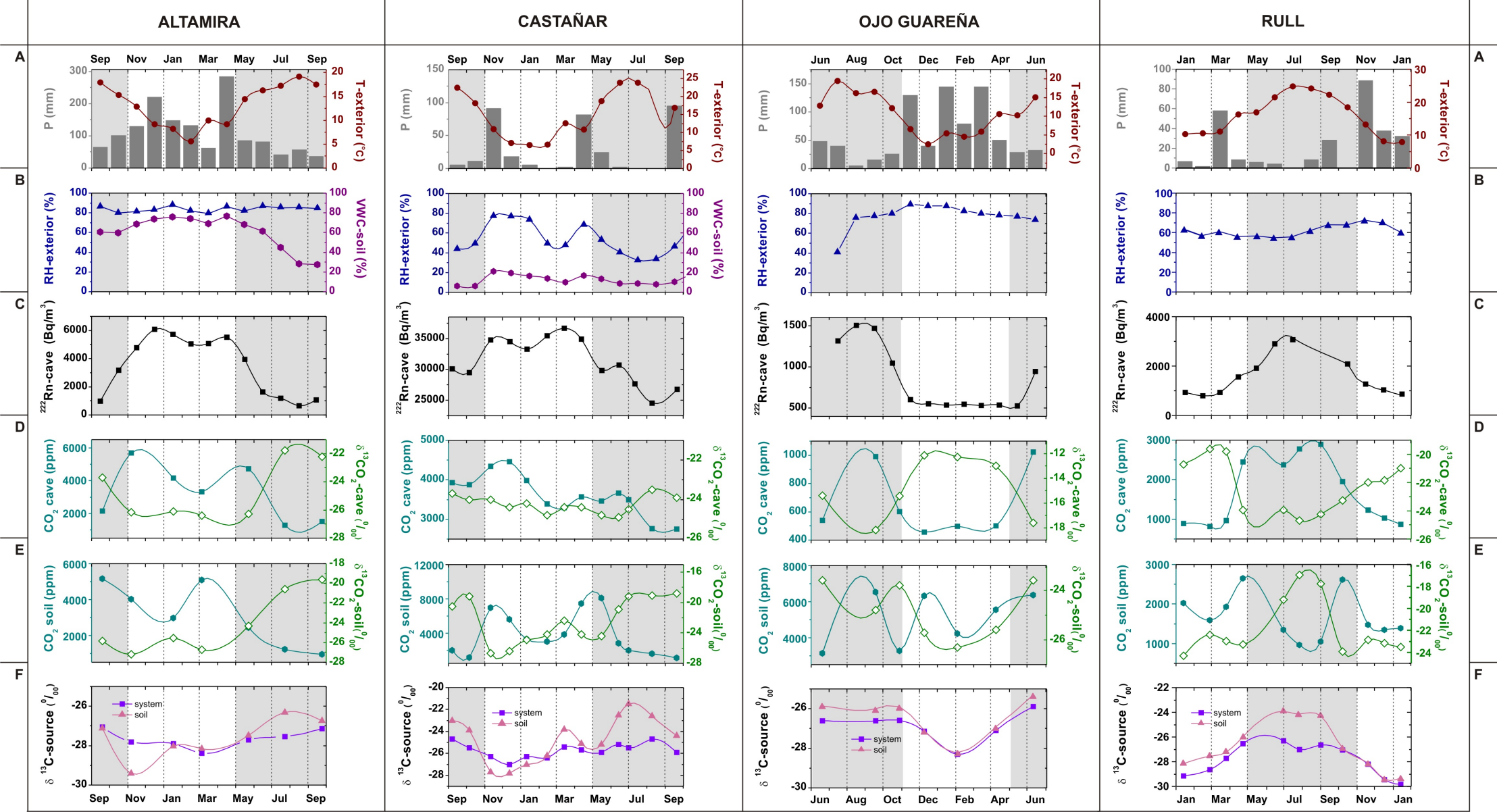
ALTAMIRA
CASTAÑAR
OJO GUAREÑA
RULL
A
B
C
D
E
F
P (mm)
T-exterior (°C)
RH-exterior (%)
VWC-soil (%)
222Rn-cave (Bq/m3)
CO2 cave (ppm)
δ13CO2-cave (‰)
CO2 soil (ppm)
δ13CO2-soil(‰)
δ13C-source (‰)
system
soil
Sep Nov Jan Mar May Jul Sep
Jun Aug Oct Dec Feb Apr Jun
Jan Mar May Jul Sep Nov Jan

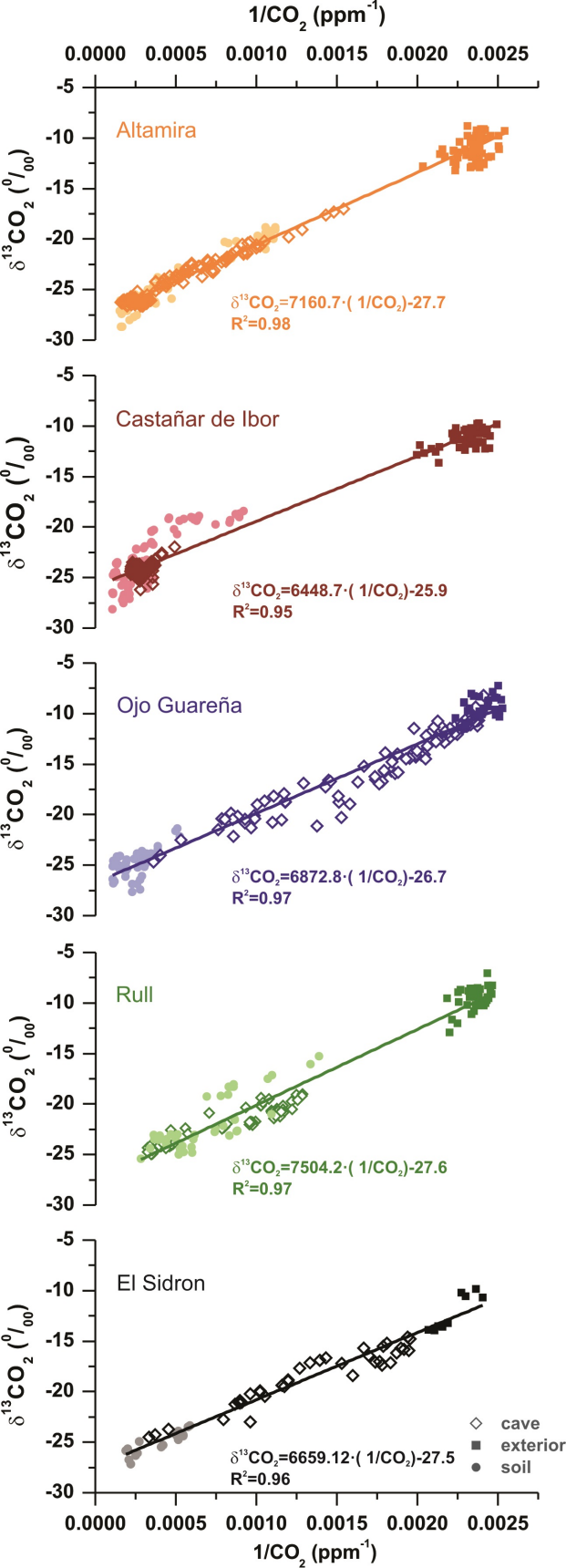
1/CO2 (ppm-1)
0.0000
0.0005
0.0010
0.0015
0.0020
0.0025
δ13CO2 (0/00)
-5
-10
-15
-20
-25
-30
Altamira
δ13CO2=7160.7·(1/CO2)-27.7
R2=0.98
Castañar de Ibor
δ13CO2=6448.7·(1/CO2)-25.9
R2=0.95
Ojo Guareña
δ13CO2=6872.8·(1/CO2)-26.7
R2=0.97
Rull
δ13CO2=7504.2·(1/CO2)-27.6
R2=0.97
El Sidron
δ13CO2=6659.12·(1/CO2)-27.5
R2=0.96
cave
exterior
soil

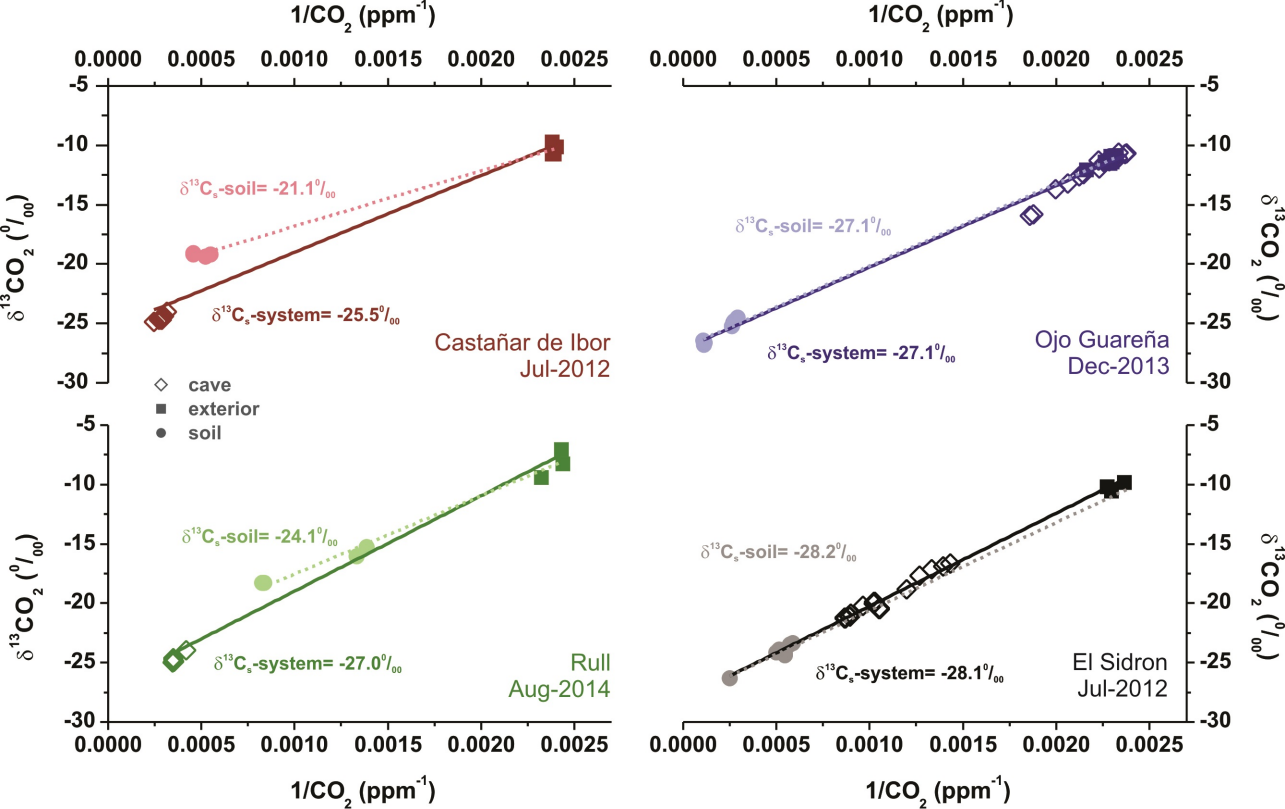
1/CO2 (ppm-1)
0.0000
0.0005
0.0010
0.0015
0.0020
0.0025
δ13CO2 (0/00)
-5
-10
-15
-20
-25
-30
δ13Cs-soil= -21.1 0/00
δ13Cs-system= -25.5 0/00
Castañar de Ibor
Jul-2012
cave
exterior
soil
δ13Cs-soil= -27.1 0/00
δ13Cs-system= -27.1 0/00
Ojo Guareña
Dec-2013
δ13Cs-soil= -24.1 0/00
δ13Cs-system= -27.0 0/00
Rull
Aug-2014
δ13Cs-soil= -28.2 0/00
δ13Cs-system= -28.1 0/00
El Sidron
Jul-2012

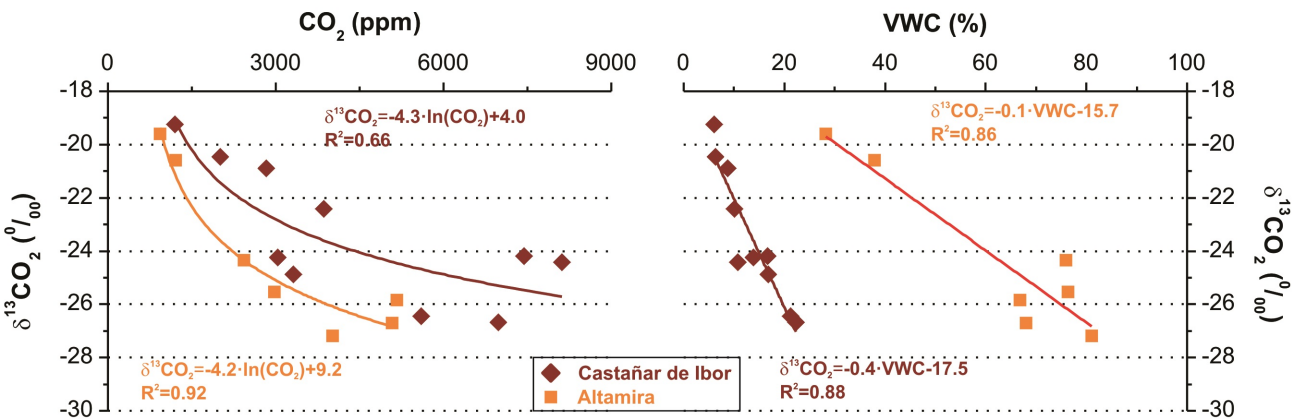
CO2 (ppm)
0
3000
6000
9000
VWC (%)
0
20
40
60
80
100
-18
-20
-22
-24
-26
-28
-30
δ13CO2 (0/00)
δ13CO2=-4.3·ln(CO2)+4.0
R2=0.66
δ13CO2=-4.2·ln(CO2)+9.2
R2=0.92
δ13CO2=-0.1·VWC-15.7
R2=0.86
δ13CO2=-0.4·VWC-17.5
R2=0.88
Castañar de Ibor
Altamira

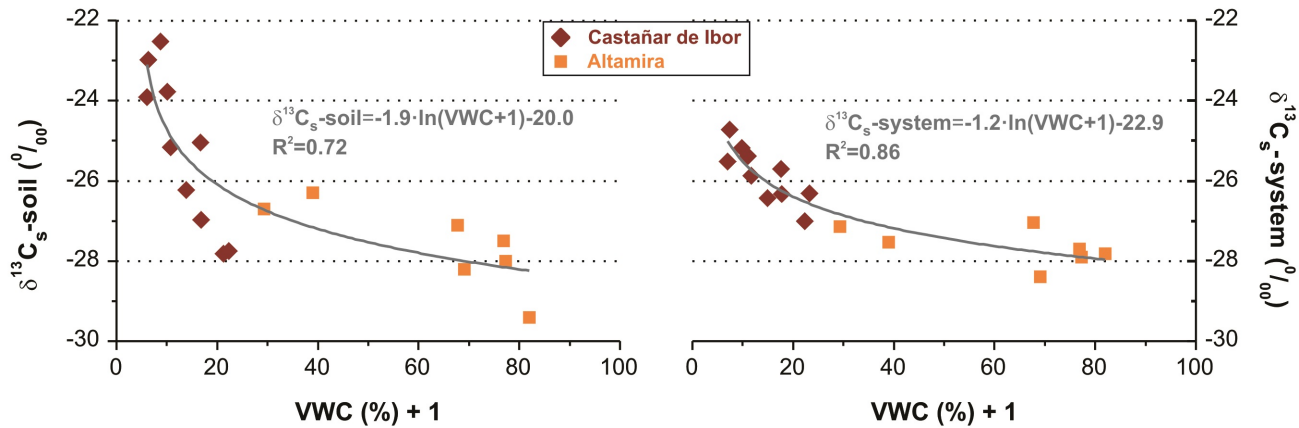
Castañar de Ibor
Altamira
δ13Cs-soil=-1.9·ln(VWC+1)-20.0
R2=0.72
δ13Cs-system=-1.2·ln(VWC+1)-22.9
R2=0.86
δ13Cs-soil (0/00)
δ13Cs-system (0/00)
VWC (%) + 1
VWC (%) + 1
-22
-24
-26
-28
-30
0
20
40
60
80
100

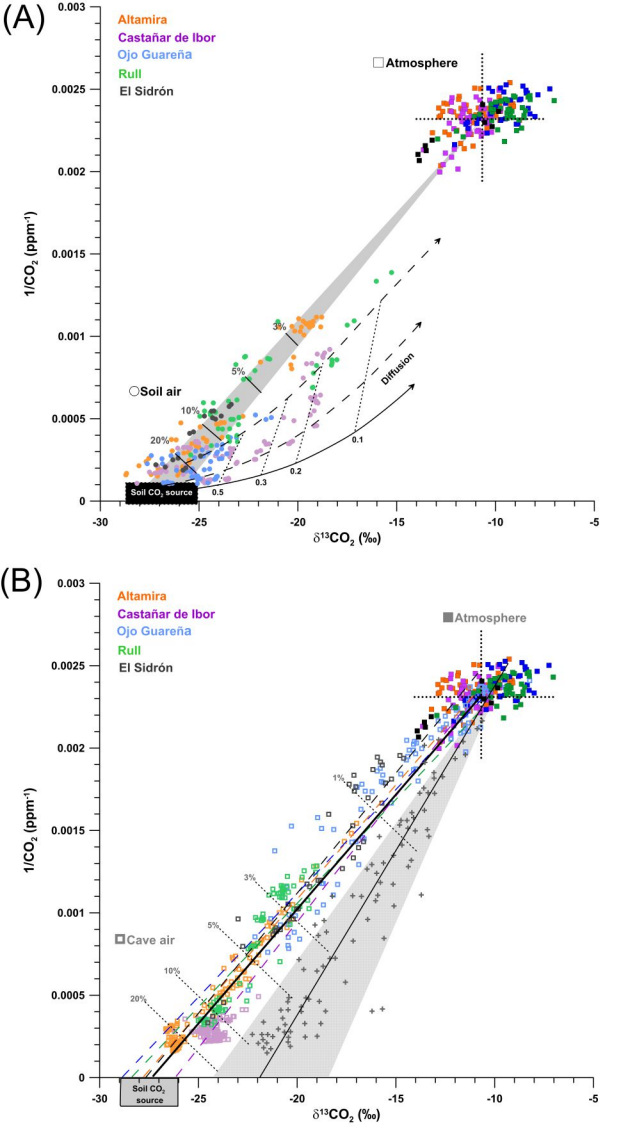
(A)
Altamira
Castañar de Ibor
Ojo Guareña
Rull
El Sidrón
Atmosphere
Soil air
Diffusion
3%
5%
10%
20%
0.1
0.2
0.3
0.5
Soil CO2 source
1/CO2 (ppm-1)
δ13CO2 (‰)
(B)
Altamira
Castañar de Ibor
Ojo Guareña
Rull
El Sidrón
Atmosphere
Cave air
1%
3%
5%
10%
20%
Soil CO2 source
1/CO2 (ppm-1)
δ13CO2 (‰)

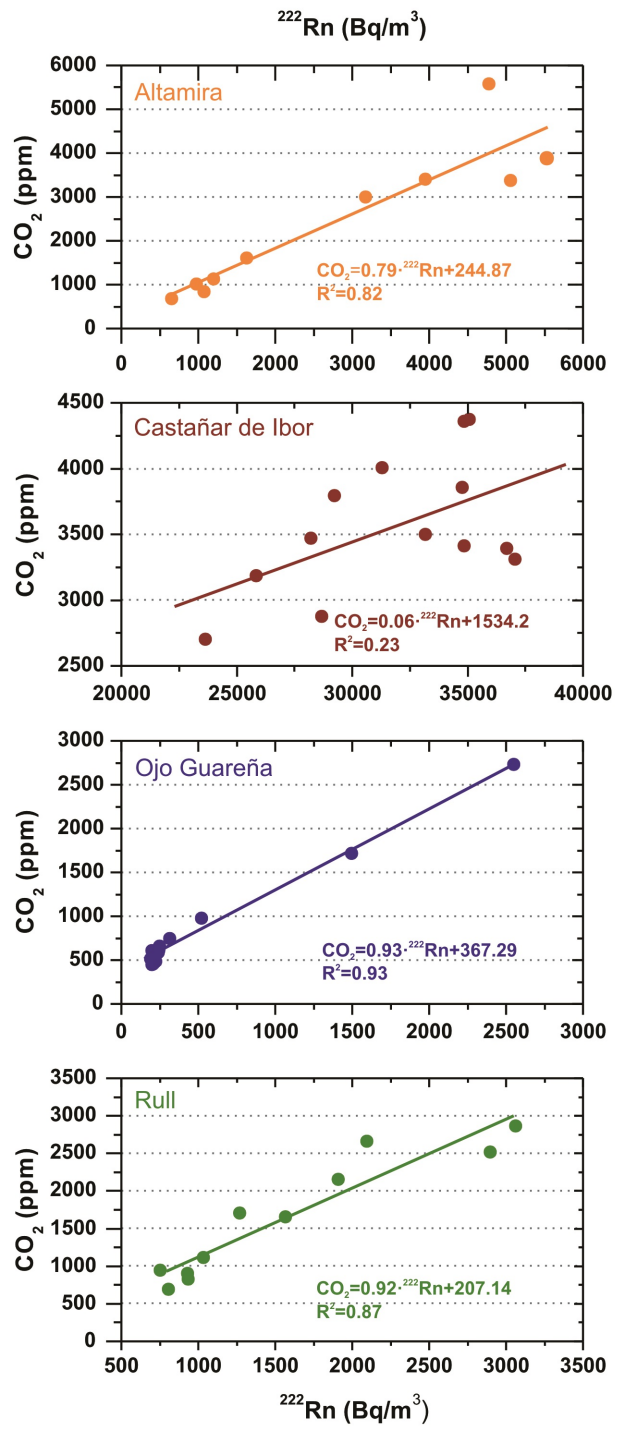
222Rn (Bq/m3)
Altamira
CO2 (ppm)
CO2=0.79·222Rn+244.87
R2=0.82
Castañar de Ibor
CO2 (ppm)
CO2=0.06·222Rn+1534.2
R2=0.23
Ojo Guareña
CO2 (ppm)
CO2=0.93·222Rn+367.29
R2=0.93
Rull
CO2 (ppm)
CO2=0.92·222Rn+207.14
R2=0.87
222Rn (Bq/m3)

Table captions

Table 1: Data summary of the main features of the studied caves (extracted from Fernandez-Cortes et al., 2015b, supplementary information). A detailed description and additional data can be found in: 1) Cuezva et al., 2009 and Cuezva et al., 2011; 2) Fernandez-Cortes et al., 2011 and Alonso-Zarza et al., 2011; 3) Camacho et al., 2006 and Fernandez-Cortes et al., 2015a; 4) Pla et al., 2015 and 5) Rosas et al., 2006 and Lalueza-Fox et al., 2011.

Table 2: Average values and ranges of variation (difference between maximum and minimum values) for the CO_2 concentration and the $\delta^{13}CO_2$ in the air. Values have been grouped according to the air mass (soil, cave or exterior air), field campaign and study site. The isotopic ratio of the source ($\delta^{13}C_s$) is also referred. This was calculated with the Keeling model for the soil ($\delta^{13}C_s$-soil) and the system ($\delta^{13}C_s$-system) for each field campaign.

Table 3: Mean values and ranges of variation for the total amount of samples collected during the annual cycles studied at each field site.

Cave	Geographic coordinates of cave entrance			Host-rock	Morphometric data			Climate: average annual data			
	latitude	longitude	altitude (m.a.s.l.)		Depth of the sampled area	Length of the sampled area	Total length	Classification	T (°C)	Rain (mm)	Cave T (°C)
Altamira[1]	43° 22' 40'' N	4° 7' 6'' W	159	Dolomitized calcarenitic limestones	3 – 22 m (average 8 m)	220 m	270 m	Oceanic or Cfb: temperate without dry season and temperate summer	13.9	1350	13.7
Castañar de Ibor[2]	39° 38' 13'' N	5° 25' 33'' W	590	Shales and greywackes with dolostones	15 – 55 m (average 25 m)	650 m	2315 m	Mediterranean or Csa: temperate with dry and hot summer	15.5	546	17.0
Ojo Guareña[3]	42° 02' N	3° 39' W	785	Limestones and dolomitic limestones	30 -80 m (average 52 m)	2.5 Km	110 Km	Oceanic or Cfb: temperate without dry season and temperate summer	10.1	778.1	10.8
Rull[4]	38° 48' 20'' N	0° 10' 38'' W	490	Limestone conglomerates	9 - 23 m (average 18 m)	46 m	46 m	Mediterranean or Csa: temperate with dry and hot summer	15.8	319	15.9
El Sidron[5]	43° 23'07'' N	5° 19' 34'' W	167	Limestone conglomerates and sandstones	5 - 35 m (average 23 m)	600 m	600 m	Oceanic or Cfb: temperate without dry season and temperate summer	13.1	1292	12.0

Location	Date	Soil					Cave					Exterior					δ^{13}Cs	
		CO_2 (ppm)		$\delta^{13}CO_2$ (‰)		N	CO_2 (ppm)		$\delta^{13}CO_2$ (‰)		N	CO_2 (ppm)		$\delta^{13}CO_2$ (‰)		N	Keeling plot intercept	
		Average	Range	Average	Range		Average	Range	Average	Range		Average	Range	Average	Range		system	soil
Altamira	Sep-11	5163.6	2335.0	-25.8	0.6	6	2163.0	2845.3	-23.7	4.3	15	420.5	97.5	-11.3	3.6	5	-27.0	-27.1
	Nov-11	4015.3	4184.0	-27.2	3.8	7	5678.0	2001.0	-26.2	0.5	19	436.1	23.9	-12.5	1.5	5	-27.8	-29.4
	Jan-12	2978.9	1242.6	-25.5	2.9	8	4151.4	1540.9	-26.1	0.9	11	424.6	8.5	-11.0	3.6	5	-27.9	-28.0
	Mar-12	5084.2	3199.9	-26.7	1.9	7	3320.8	656.4	-26.4	0.6	16	412.7	23.4	-11.6	2.9	9	-28.4	-28.2
	May-12	2434.7	898.8	-24.3	1.6	8	4727.2	942.2	-26.3	0.9	9	426.0	49.4	-9.7	2.3	11	-27.7	-27.5
	Jul-12	1213.9	1020.6	-20.6	3.9	8	1277.4	1727.1	-21.8	7.1	23	435.1	54.4	-10.4	2.5	7	-27.5	-26.3
	Sep-12	935.5	96.5	-19.6	1.5	14	1518.9	1855.7	-22.2	7.8	24	434.7	30.7	-11.3	1.9	13	-27.1	-26.7
Castañar de Ibor	Sep-11	2012.6	75.8	-20.5	0.5	2	3933.1	151.6	-23.7	0.2	5	411.3	20.8	-10.7	1.8	2	-24.7	-23.0
	Oct-11	1192.9	227.5	-19.2	1.1	4	3874.0	172.1	-24.0	0.4	11	468.2		-12.1		1	-25.5	-23.9
	Nov-11	6981.7	4889.3	-26.7	2.5	8	4341.1	286.5	-24.0	0.8	12	444.7	48.7	-12.6	2.1	2	-26.3	-27.7
	Dec-11	5595.1	1335.5	-26.4	2.2	15	4457.6	237.2	-24.4	0.5	12	437.2	18.0	-10.3	0.2	3	-27.0	-27.8
	Jan-12	3312.0	663.7	-24.9	2.6	10	3985.8	469.9	-24.2	1.1	12	464.0	64.4	-11.7	0.5	2	-26.3	-27.0
	Feb-12	3036.1	682.1	-24.2	1.9	8	3387.7	491.2	-24.8	0.5	12	410.6	7.8	-11.6	1.2	3	-26.4	-26.2
	Mar-12	3859.3	1120.5	-22.4	1.2	6	3291.4	139.4	-24.4	0.8	11	423.6	38.5	-11.4	1.9	6	-25.4	-23.8
	Apr-12	7445.1	544.3	-24.2	1.4	8	3565.5	121.5	-24.4	1.3	10	438.0	29.6	-10.4	1.1	4	-25.7	-25.1
	May-12	8116.1	1725.4	-24.4	1.3	12	3466.2	252.9	-24.8	0.5	12	435.8	53.7	-11.3	2.0	10	-25.9	-25.2
	Jun-12	2834.1	141.8	-20.9	1.4	7	3663.1	302.1	-24.9	1.7	12	428.6	12.0	-11.9	0.7	4	-25.2	-22.5
	Jul-12	2029.0	369.8	-19.2	0.3	4	3493.3	868.5	-24.5	0.8	12	418.4	3.6	-10.3	1.0	4	-25.5	-21.5
	Aug-12	1621.8	125.3	-19.1	0.5	8	2765.2	888.2	-23.5	3.0	11	438.0	17.2	-10.7	0.4	5	-24.7	-22.6
	Sep-12	1139.5	110.3	-18.8	0.9	5	2750.5	533.1	-23.9	3.1	12	457.3	75.2	-11.6	2.5	7	-25.9	-24.4
Ojo Guareña	Jun-13	3119.1	1986.1	-23.6	1.9	6	538.8	304.8	-15.4	9.9	14	399.1	6.9	-9.8	0.9	4	-26.6	-25.8
	Sep-13	6524.3	2393.6	-24.8	0.6	5	989.1	2361.4	-18.2	15.2	15	411.6	15.7	-8.4	0.0	2	-26.6	-26.0
	Oct-13	3276.5	1568.8	-23.8	1.3	6	601.7	748.4	-15.4	11.7	15	407.3	35.8	-9.1	1.7	5	-26.6	-25.9
	Dec-13	6330.2	5852.0	-25.7	2.3	8	457.7	116.9	-12.1	5.3	17	440.5	31.5	-11.4	1.2	6	-27.1	-27.1
	Feb-14	4234.8	2435.5	-26.3	2.8	8	496.8	485.4	-12.3	10.5	15	417.3	14.7	-9.8	1.0	6	-28.3	-28.2
	Apr-14	5543.6	3332.1	-25.6	1.4	8	502.2	144.4	-13.0	7.6	15	423.7	37.8	-9.4	1.7	6	-27.1	-26.9
	Jun-14	6370.7	7469.9	-23.6	3.7	8	1023.3	2074.7	-17.6	15.8	16	422.2	37.4	-8.2	1.7	6	-25.9	-25.3
Rull	Jan-14	2023.4	436.6	-24.3	1.1	6	892.0	54.6	-20.7	0.5	13	414.0	16.8	-9.4	1.8	7	-29.1	-28.2
	Feb-14	1586.7	860.3	-22.4	2.0	4	814.4	82.0	-19.6	1.5	7	421.0	37.4	-9.3	1.6	4	-28.6	-27.6
	Mar-14	1925.9	926.6	-23.0	1.0	3	964.2	48.5	-19.8	0.8	5	429.2	5.1	-8.9	0.7	3	-27.7	-27.2
	Apr-14	2654.3	262.1	-23.3	0.5	4	2453.2	52.9	-23.9	0.6	5	427.2	14.4	-9.3	1.5	3	-26.6	-26.0
	Jul-14	1350.8	235.6	-19.2	0.2	4	2376.9	416.0	-23.9	0.7	6	433.4	37.7	-9.1	1.1	3	-26.3	-23.9
	Aug-14	968.5	491.2	-17.0	3.0	4	2777.6	505.2	-24.7	1.0	6	417.4	20.0	-8.2	2.4	3	-27.0	-24.1
	Sep-14	1045.9	252.5	-17.7	1.1	4	2890.2	959.6	-24.2	2.2	7	438.7	15.1	-8.7	0.4	3	-26.6	-24.3
	Oct-14	2622.5	1606.7	-23.9	2.4	4	1949.0	868.1	-23.3	3.5	7	430.9	32.9	-10.3	2.3	3	-27.0	-26.9
	Nov-14	1473.7	386.5	-22.9	1.3	4	1230.5	202.7	-22.0	2.1	7	413.2	14.1	-9.6	1.0	3	-28.2	-28.1
	Dec-14	1352.4	760.6	-23.2	3.8	4	1033.7	41.4	-21.8	0.4	7	423.2	13.5	-10.7	0.8	3	-29.5	-29.4
	Jan-15	1393.4	685.8	-23.5	2.0	3	869.8	84.1	-21.0	0.9	6	440.3	34.4	-11.7	2.7	3	-29.8	-29.3
El Sidron	Sep-11	4528.2	1665.9	-26.1	2.3	6	1368.5	2444.5	-20.9	9.0	11	445.2	48.0	-12.5	2.9	3	-27.4	-27.6
	Jan-12	2183.4	494.6	-25.0	1.2	4	552.9	114.1	-16.2	3.8	14	476.4	13.7	-13.8	0.4	3	-28.1	-28.1
	Jul-12	2150.4	2293.3	-24.3	3.0	7	941.4	456.1	-19.4	4.6	13	432.6	17.2	-10.2	0.7	3	-28.1	-28.2

Location	Sampling period	Soil					Cave					Exterior				
		CO_2 (ppm)		$\delta^{13}CO_2$ (‰)		N	CO_2 (ppm)		$\delta^{13}CO_2$ (‰)		N	CO_2 (ppm)		$\delta^{13}CO_2$ (‰)		N
		Average	Range	Average	Range		Average	Range	Average	Range		Average	Range	Average	Range	
Altamira	sept 2011-sept2012	2773.2	5686.8	-23.6	9.9	58	2969.5	5566.8	-24.2	9.7	117	427.2	97.5	-11.0	4.4	55
Castañar de Ibor	sept 2011-sept 2012	4461.0	8374.9	-23.3	9.8	97	3604.9	2537.2	-24.3	4.3	144	435.5	99.7	-11.2	3.9	53
Ojo Guareña	jun 2013-jun 2014	5119.0	7528.9	-24.9	6.3	49	659.3	2368.6	-14.8	16.5	107	419.4	66.3	-9.5	4.8	35
Rull	jan 2014-jan 2015	1689.0	2854.4	-21.9	10.2	44	1582.3	2330.4	-22.1	6.0	76	424.8	51.8	-9.5	5.9	38
El Sidron	sept 2011-jul 2012	2997.4	3616.2	-25.1	3.8	17	921.9	2492.5	-18.7	9.9	38	451.4	68.3	-12.1	4.1	9